Engineering Structures 228 (2021) 111550

Contents lists available at ScienceDirect

Engineering Structures

journal homepage: www.elsevier.com/locate/engstruct

Simplified multimode control of seismic response of high-rise chimneys using distributed tuned mass inerter systems (TMIS)

Li Zhang [a,b], Songtao Xue [b,c], Ruifu Zhang [a,b,*], Liyu Xie [b], Linfei Hao [d]

[a] State Key Laboratory of Disaster Reduction in Civil Engineering, Tongji University, Shanghai 200092, China
[b] Department of Disaster Mitigation for Structures, Tongji University, Shanghai 200092, China
[c] Department of Architecture, Tohoku Institute of Technology, Sendai 982-8577, Japan
[d] Earthquake Engineering Research & Test Center, Guangzhou University, Guangzhou 510405, China

ARTICLE INFO

Keywords:
Chimney
Tuned mass inerter system
Ungrounded
Multimode
Vibration control
Lightweight

ABSTRACT

The industrial chimney is one of the important components used in industrial processes. The tuned mass damper was introduced in previous studies to improve its reliability for resisting earthquakes. However, a large additional mass is generally required for applying a tuned mass damper in a chimney, which may be inappropriate owing to the additional moment action. In this study, the tuned mass inerter system (TMIS) is adopted as an ungrounded lightweight passive control device for the seismic response mitigation of high-rise chimneys. The ungrounded TMIS consists of a tuned mass element and a parallel-connected tuning spring and inerter subsystem. Considering that the influence of high modes on the responses of a high-rise chimney may not be neglected, distributed TMISs (d-TMISs) are proposed for installation on the chimney for multimode control of seismic response. A strategy to optimize d-TMISs for multimode control of high-rise chimneys is developed. A typical numerical chimney model is established to illustrate the proposed optimal design method. Time history analysis and comparative studies are conducted to verify the optimal multimode control design and the lightweight effect of d-TMISs compared to the traditional tuned mass dampers. The results show that by applying the proposed optimization in d-TMISs, the performance objectives can be achieved and the chimney's responses involving the high-order modes can be reduced as anticipated. The required weight of d-TMISs is less than that for tuned mass dampers under an identical performance objective. It is observed that the proposed optimal multimode control method is effective and that d-TMISs can achieve the lightweight effect.

1. Introduction

Industrial chimneys are tall and slender structures that are used for discharging the flue gases generated by entities including the electrical and petrochemical industries [1,2]. From the perspective of structural characteristics, typical high-rise chimneys (whose heights range from 100 m to 420 m [3]) are considered to be vulnerable under horizontal loads (earthquake and wind excitations) [4–8]. On August 17, 1999, a 115 m reinforced concrete (RC) chimney collapsed under the Marmara earthquake [9]. During the 2007 Niigata-ken Chuetsu-oki earthquake, a RC chimney was structurally damaged owing to the influence of a long-period earthquake, according to the analytical results [10]. Because chimneys are an important part of industrial processes, damage to these during earthquakes can cause severe consequences in terms of both economic loss and threat to human life.

Various methods or devices are adopted to design or retrofit chimneys and thereby enhance the safety redundancy of these high-rise structures. Wilson [11] presented a nonlinear dynamic analysis procedure for RC chimneys, based on experimental results. Furthermore, they recommended the development of ductility to dissipate seismic energy and prevent brittle failure of chimneys. However, the excessive development of structural nonlinear behavior may damage the primary structure, which is not convenient to repair. To resolve this problem, passive control devices are mounted on chimneys to mitigate their vibration responses. Brownjohn et al. [12] reported the effectiveness of the tuned mass damper (TMD) for vibration control of a 183 m chimney according to the response data of a real-time performance monitoring system. Using finite element analysis, Longarini and Zucca [13] demonstrated that the seismic performance of an existing chimney can be improved effectively by installing TMD. High modes may exert an

* Corresponding author at: State Key Laboratory of Disaster Reduction in Civil Engineering, Tongji University, Shanghai 200092, China.
E-mail address: zhangruifu@tongji.edu.cn (R. Zhang).

https://doi.org/10.1016/j.engstruct.2020.111550
Received 22 June 2020; Received in revised form 5 November 2020; Accepted 8 November 2020
Available online 5 December 2020

appreciable influence on the dynamic responses of high-rise chimneys under seismic excitations [11,14,15]. Elias et al. [3,16] conducted multimode control using distributed TMDs mounted along the height of an RC chimney, to obtain better dynamic response mitigation compared with that obtained by a single mode control. However, the application of traditional TMD generally requires the determination of a certain mass ratio (e.g., from 1% to 5%) of the total mass of the primary structure [17,18], which may be relatively large for high-rise chimneys considering the additional moment action, particularly for the retrofitting scenario.

Recently, the inerter was introduced and demonstrated to be effective for structural vibration control [19–21]. It exhibits an apparent mass effect through the transformation of motion with a small gravitational mass. The applications of inerters have been of interest to scholars for different types of civil structures such as multistory buildings [22–28], storage tanks [29–31], wind turbine towers [32,33] and bridges [34]. The inerter can be considered as a two-terminal inertia element whose reaction force is proportional to the relative acceleration of its two ends [35]. The utilization of a two-terminal inertia element can be traced back to the 1970 s, when Kawamata [36,37] proposed a mass pump to utilize the inertance of a fluid based on the hydraulic mechanism. Saito et al. [38] and Ikago et al. [21,39] proposed the tuned viscous mass damper (TVMD) by employing the ball screw mechanism to transform linear motion into a rapid rotation of a flywheel and by incorporating tuning spring and viscous damping. In addition, they experimentally demonstrated the effectiveness of the TVMD in structural response mitigation, and presented the apparent mass and damping enhancement effects of the TVMD for the first time. The TVMD can be considered as an inerter system. A few scholars recommend the application of the well-known fixed-point theory for designing an inerter system [21,40]. However, the inherent damping of the primary structure is omitted in this technology. Pan et al. [19] proposed a demand-oriented design method for a structure with a TVMD. Hereby, they considered the inherent damping coefficient of the primary structures and the trade-off between the structural responses and cost. The theoretical essence of damping enhancement mechanism of inerter systems is not clear in previous studies. Zhang et al. [41] discovered and proved the damping enhancement equation of inerter systems, and revealed the theoretical essence of inerter systems. To directly use the damping enhancement mechanism of inerter systems, a design method based on the damping enhancement equation is also proposed by them. Inspired by the characteristics of inerters with improved performance, inerter-based systems composed of different topology layouts have been proposed and researched for civil structures. As a variant of TVMD, tuned inerter damper was presented by Lazar et al. [42] for suppressing structural vibration responses by connecting the inerter element in series with a parallel-connected spring and damping element. Pan and Zhang [35] derived the closed-form expressions of the root mean square (RMS) responses of an SDOF model incorporating the typical inerter systems with different mechanical layouts under stochastic excitations. In addition, they proposed the corresponding direct design method. The structural vibration control effects for the inerter-based systems with different layouts were also analyzed under optimized objectives by Xue et al. [43], Zhao et al. [44], Krenk [45], and Javidialesaadi and Wierschem [46].

By substituting the damping element of the TMD with a TVMD, Garrido et al. [47] suggested the rotational inertia double-tuned massed damper (RIDTMD) for vibration control of civil engineering structures. The RIDTMD is demonstrated to be more efficient than the TMD for an identical mass ratio, particularly near the resonance frequency. Zhang and his coworkers [32,48] proposed several ungrounded tuned mass inerter systems (TMISs) with the objective of lightweight tuning mass, including the tuned inerter mass system (TIMS) for suppressing the vibration of floors under human-induced excitation and tuned parallel inerter mass system (TPMIS) for reducing the responses of wind turbine towers. By connecting the inerter with TMD, De Domenico and Ricciardi [49] proposed the grounded tuned mass damper inerter (TMDI) used in isolation system with a better robustness. In addition, the tuned liquid inerter system (TLIS) are proposed by Zhao et al. [50] for mitigating oscillatory motion. Although many studies have been conducted on the application of inerter-based passive control devices in structures, further study is required to investigate the effectiveness of these devices in high-rise structures, such as tall and slender chimneys. The utilization of lightweight devices can be favorable for their convenient installation and for the reduction of additional moment action of chimneys. As a tower-type structure similar to a chimney, the slender wind turbine tower has been investigated using TPMIS with the objective of attaining a lightweight effect [32]. However, only the first mode is controlled with a TPMIS installed at the top of the wind turbine tower. The vibration suppression of high-rise chimneys under seismic excitation may involve a multimode control approach. Several vibration control devices may be required for multimode control of the seismic response of a chimney. The corresponding design method needs to be developed considering the performance demand, which requires further research.

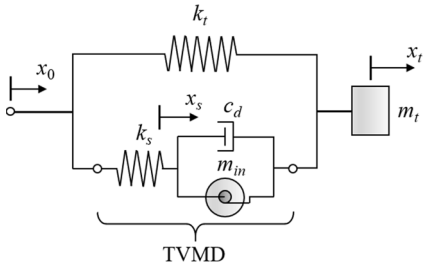

Fig. 1. Model of the TMIS.

In this study, a lightweight vibration mitigation device, the ungrounded TMIS, is adopted for mitigating the seismic response of a high-rise chimney. The TMIS is composed of a tuned mass element and a parallel-connected tuning spring and inerter subsystem. The high-rise chimney equipped with distributed TMISs (d-TMISs) is investigated for multimode control of seismic response. This is conducted considering that the influence of high modes may play an important role in the seismic responses of the chimneys. A multimode optimization control method based on demand-based seismic design is proposed for the high-rise chimney with d-TMISs. A typical RC chimney model is established to illustrate the proposed optimal design method. Time history analysis and comparative studies are conducted to verify the effectiveness of the proposed design and the lightweight effect of d-TMISs compared to the traditional distributed TMDs (d-TMDs). In addition, parametric studies are performed on the d-TMISs used for multimode control of the seismic responses of the chimneys.

The paper is structured as follows: Section 2 describes the mechanical model of ungrounded TMIS and the RC chimney with d-TMIS. It also presents the calculation of the corresponding stochastic responses. Section 3 presents the determination of the location of the d-TMISs used for multimode control of the chimney and the simplification of certain parameters of d-TMISs. Then, the optimal strategy for multimode

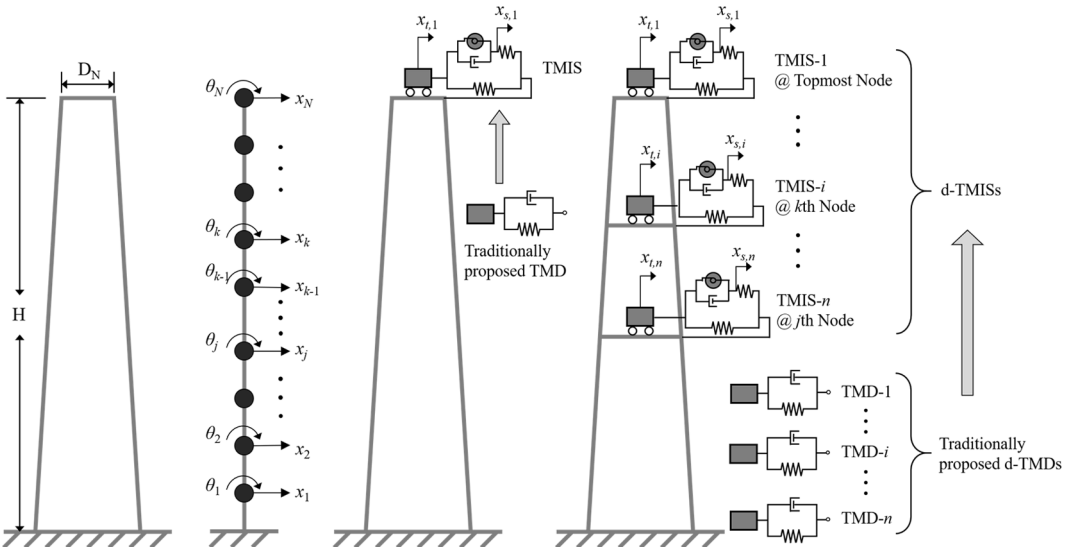

Fig. 2. Models of chimney: (a) uncontrolled model; (b) lumped mass model; (c) chimney with a single TMIS; (d) chimney with distributed TMISs.

control of the seismic response of the chimney using d-TMISs and the corresponding design steps are proposed. Section 4 presents a case study on the proposed optimal multimode control of the chimney using d-TMISs and presents the lightweight effect of d-TMISs compared to traditional d-TMDs. Section 5 presents parametric studies. The conclusions are presented in Section 6. The main subject of the study is the lightweight effect of d-TMISs and their multimode control effect on high-rise chimneys when the proposed optimal multimode control strategy is adopted.

2. Modeling and basic theory

2.1. TMIS

A schematic representation of the ungrounded TMIS is depicted in Fig. 1, which was reported in [32,47] for structural vibration control. The TMIS is developed by replacing the damping element of a traditional TMD with a TVMD [35], as shown in Fig. 1. In the TVMD, the inerter and damping elements are connected in parallel, and then they are together connected to the spring element in series. The inerter element in this inerter subsystem provides the mass enhancement and facilitates the lightweight effect of the TMIS compared with the traditional TMD [48]. Additionally, unlike the damping element used in the TMD for energy dissipation, the TVMD in the TMIS can both absorb and dissipate the external input energy, and a more sufficient energy dissipation effect can be achieved [32]. Hence, the additional ungrounded TMIS in the structure is expected to obviously improve the structural performance with a lightweight device [47]. The definitions of main symbols adopted in this study are presented in Table A1 of Appendix A.

In the TMIS shown in Fig. 1, the parameters k_t and k_s are the stiffnesses of the tuning spring and the spring element in the TVMD, respectively; c_d is the damping coefficient; m_t denotes the tuned mass; and m_{in} is referred to as the inertance of the inerter element. The displacements of the tuned mass, the end of the spring and the installation node of the TMIS are denoted as x_t, x_s and x_0, respectively. For the two-terminal inerter element in the TMIS, the output force F_{in}, which is proportional to the relative acceleration of its two nodes, can be calculated as

$$F_{in} = m_{in}\left(\ddot{x}_t - \ddot{x}_s\right) \tag{1}$$

In the TMIS, the force F_s of the inerter subsystem can be expressed as

$$F_s = m_{in}\left(\ddot{x}_t - \ddot{x}_s\right) + c\left(\dot{x}_t - \dot{x}_s\right) = k_s(x_s - x_0) \tag{2}$$

The total output force F_t of the TMIS can be calculated as

$$F_t = F_s + k_t(x_t - x_0) = -m_t\ddot{x}_t \tag{3}$$

2.2. Mechanical model of a high-rise chimney with distributed TMISs

The typical high-rise chimney (Fig. 2a) [3] is checked herein for seismic response mitigation using the TMIS. An assemblage of two-dimensional (2D) beam elements with sway degrees of freedom (DOF) at each node is adopted to simulate the chimney, as shown in Fig. 2b. To reasonably simplify the calculation, the rotational DOF θ_k is condensed to build the matrices of the chimney model, and each of the beam elements is assumed to have the same cross-section throughout its height. For the uncontrolled chimney, the governing equations of motion under the ground motion excitations can be written as

$$\boldsymbol{M}_{\mathrm{p}}\ddot{\boldsymbol{x}} + \boldsymbol{C}_{\mathrm{p}}\dot{\boldsymbol{x}} + \boldsymbol{K}_{\mathrm{p}}\boldsymbol{x} = -\boldsymbol{M}_{\mathrm{p}}\boldsymbol{\iota}_{\mathrm{p}}\ddot{x}_g \tag{4}$$

where $\boldsymbol{M}_{\mathrm{p}}$, $\boldsymbol{C}_{\mathrm{p}}$, and $\boldsymbol{K}_{\mathrm{p}}$ are the condensed mass, damping and stiffness matrices of the uncontrolled chimney, respectively; $\boldsymbol{x} = \{x_1 \quad x_2 \quad \cdots \quad x_N\}^T$, $\dot{\boldsymbol{x}}$ and $\ddot{\boldsymbol{x}}$ are the vectors of the nodal displacement, velocity and acceleration of the uncontrolled chimney relative to the ground; $\boldsymbol{\iota}_{\mathrm{p}} = \{1 \quad 1 \quad \cdots \quad 1\}^T$ is the influence coefficient vector; and $\ddot{x}_g$ represents the acceleration of the ground motion. The condensed mass matrix $\boldsymbol{M}_{\mathrm{p}}$ is obtained by simply removing the inertial masses with respect to the rotation at each node of the chimney model. The stiffness matrix $\boldsymbol{K}_{\mathrm{p}}$ is built with the static condensation of rotational DOF. These two matrices can be expressed as follows:

$$\boldsymbol{M}_{\mathrm{p}}=\begin{bmatrix} m_1 & & & & \\ & \ddots & & & \\ & & m_k & & \\ & & & \ddots & \\ & & & & m_N \end{bmatrix}_{N\times N} \tag{5}$$

$$\boldsymbol{K}_{\mathrm{p}}^{*}=\begin{bmatrix} \boldsymbol{K}_{\mathrm{T}} & \boldsymbol{K}_{\mathrm{T}\theta} \\ \boldsymbol{K}_{\theta\mathrm{T}} & \boldsymbol{K}_{\theta} \end{bmatrix} \rightarrow \mathbf{K}_{\mathrm{p}}=\mathbf{K}_{\mathrm{T}}-\mathbf{K}_{\mathrm{T}\theta}\mathbf{K}_{\theta}^{-1}\mathbf{K}_{\theta\mathrm{T}} \tag{6}$$

where m_k denotes the lumped mass at the k^{th} node of the chimney model; $\boldsymbol{K}_{\mathrm{T}}$ and $\boldsymbol{K}_{\theta}$ are the stiffness matrices with respect to the translational displacement and rotation, respectively. In this study, the damping matrix $\boldsymbol{C}_{\mathrm{p}}$ of the chimney is calculated by assuming the uniform damping ratio for all modes.

To mitigate the seismic response of the high-rise chimney, the TMIS is adopted in this study as a lightweight device. A single TMIS (s-TMIS) mounted on top of the chimney (Fig. 2c) can be suitable to control the structural response, which is mainly attribute to the first vibration mode. However, for the high-rise chimney, the contribution of high vibration modes to the structural response may not be neglected [14,15]. Hence, the distributed TMISs (d-TMISs) are adopted to reduce the responses in the first few modes of the chimney, as shown in Fig. 2d. Note that no more than one TMIS is installed on a node and that one TMIS is just adopted for a specified modal control of the chimney. That is, the i^{th} TMIS is adopted to control the i^{th} mode of the chimney. The locations of the d-TMISs are determined by the mode shape, which is introduced in Section 3. According to the dynamic equilibrium approach, the equations of motion of the chimney with d-TMISs under seismic excitations can be written as follows:

$$\boldsymbol{M}\ddot{\boldsymbol{X}}+\boldsymbol{C}\dot{\boldsymbol{X}}+\boldsymbol{K}\boldsymbol{X}=-\boldsymbol{M}_{g}\boldsymbol{\iota}\ddot{x}_{g} \tag{7}$$

where $\boldsymbol{M}$, $\boldsymbol{C}$, $\boldsymbol{K}$ and $\boldsymbol{M}_g$ are the mass, damping, and stiffness matrices of the chimney with d-TMISs and the mass matrix corresponding to the ground motions, respectively; $\boldsymbol{X}$, $\dot{\boldsymbol{X}}$ and $\ddot{\boldsymbol{X}}$ are the vectors of the displacement, velocity and acceleration of the chimney with d-TMISs, respectively; $\boldsymbol{\iota}$ is the influence coefficient vector of the chimney with d-TMISs. Let $x_{s,i}$ and $x_{t,i}$ represent the displacement of the end of the spring and the tuned mass relative to the ground in the i^{th} TMIS installed on the chimney; the matrices and vectors in Eq. (7) can be written as follows:

$$\boldsymbol{M}=\begin{bmatrix} \boldsymbol{M}_{\mathrm{p}} & \mathbf{0} \\ \mathbf{0} & \boldsymbol{M}_{\mathrm{I}} \end{bmatrix}_{(N+2n)\times(N+2n)},\text{where}\mathbf{M}_{\mathrm{I}}=\begin{bmatrix} m_{in,1}+m_{t,1} & -m_{in,1} & \cdots & 0 & 0 \\ -m_{in,1} & m_{in,1} & \vdots & \vdots & \\ \vdots & \ddots & & & \\ 0 & \cdots & m_{in,n}+m_{t,n} & -m_{in,n} & \\ 0 & \cdots & -m_{in,n} & m_{in,n} & \end{bmatrix}_{2n\times 2n} \tag{8}$$

$$\boldsymbol{C}=\begin{bmatrix} \boldsymbol{C}_{\mathrm{p}} & \mathbf{0} \\ \mathbf{0} & \boldsymbol{C}_{\mathrm{d}} \end{bmatrix}_{(N+2n)\times(N+2n)},\text{where }\mathbf{C}_{\mathrm{d}}=\begin{bmatrix} c_{d,1} & -c_{d,1} & \cdots & 0 & 0 \\ -c_{d,1} & c_{d,1} & \vdots & \vdots & \\ \vdots & \ddots & & & \\ 0 & \cdots & c_{d,n} & -c_{d,n} & \\ 0 & \cdots & -c_{d,n} & c_{d,n} & \end{bmatrix}_{2n\times 2n} \tag{9}$$

$$\boldsymbol{K}=\begin{bmatrix} \boldsymbol{K}_{\mathrm{p}}+\boldsymbol{K}_{\mathrm{I}11} & \boldsymbol{K}_{\mathrm{I}12} \\ \boldsymbol{K}_{\mathrm{I}21} & \boldsymbol{K}_{\mathrm{I}22} \end{bmatrix}_{(N+2n)\times(N+2n)},\text{where}$$

$$\boldsymbol{K}_{\mathrm{I}11}=[\chi_1 \ \cdots \ \chi_n]_{N\times n}\begin{bmatrix} k_{t,1}+k_{s,1} & \cdots & 0 \\ \vdots & \ddots & \vdots \\ 0 & \cdots & k_{t,n}+k_{s,n} \end{bmatrix}_{n\times n}\begin{bmatrix} \chi_1 \\ \vdots \\ \chi_n \end{bmatrix}_{n\times N};$$

$$\boldsymbol{K}_{\mathrm{I}12}=[\chi_1 \ \chi_1 \ \cdots \ \chi_n \ \chi_n]_{N\times 2n}\begin{bmatrix} -k_{t,1} & & \cdots & & 0 \\ & -k_{s,1} & & & \\ \vdots & & \ddots & & \vdots \\ & & & -k_{t,n} & \\ 0 & & \cdots & & -k_{s,n} \end{bmatrix}_{2n\times 2n};$$

$$\boldsymbol{K}_{\mathrm{I}21}=\boldsymbol{K}_{\mathrm{I}12}^{T};\mathbf{K}_{\mathrm{I}22}=\begin{bmatrix} k_{t,1} & & \cdots & 0 \\ & k_{s,1} & & \\ \vdots & & \ddots & \vdots \\ & & k_{t,n} & \\ 0 & & \cdots & k_{s,n} \end{bmatrix}_{2n\times 2n} \tag{10}$$

$$\mathbf{M}_{\mathbf{g}}=\begin{bmatrix} \mathbf{M}_{\mathbf{p}} & \mathbf{0} \\ \mathbf{0} & \mathbf{M}_{\mathbf{T}} \end{bmatrix}_{(N+2n)\times(N+2n)},\text{where }\mathbf{M}_{\mathbf{T}}=\begin{bmatrix} m_{t,1} & 0 & \cdots & 0 & 0 \\ 0 & 0 & & \vdots & \vdots \\ \vdots & & \ddots & & \\ 0 & \cdots & & m_{t,n} & 0 \\ 0 & \cdots & & 0 & 0 \end{bmatrix}_{2n\times 2n} \tag{11}$$

$$\boldsymbol{X}=\{x_1 \ x_2 \ \cdots \ x_N \ x_{t,1} \ x_{s,1} \ \cdots \ x_{t,i} \ x_{s,i} \ \cdots \ x_{t,n} \ x_{s,n}\}^{T} \tag{12}$$

$$\boldsymbol{\iota}=\{\boldsymbol{\iota}_{\mathrm{p}}^{T} \ 1 \ 0 \ \cdots \ 1 \ 0 \ \cdots \ 1 \ 0\}^{T} \tag{13}$$

For the description of $\boldsymbol{K}$ in Eq. (10), χ_i is the column vector representing the location of the i^{th} TMIS, which is defined as the vector of zeros with its k^{th} entry being one which specifies the node that the i^{th} TMIS is connected to in the chimney model, as shown in Fig. 2d.

2.3. Calculation of stochastic responses

The seismic design of civil structures usually needs to appropriately describe the stochastic characteristics of the seismic excitation. In this study, the high-rise RC chimney is exposed to earthquake excitations represented by stochastic processes. For the structural control, the ground motion $\ddot{x}_g$ is assumed as a zero-mean Gaussian white noise with a power spectral density (PSD) of $S(\Omega)=S_0$, where Ω is the frequency of the external excitation [35,51]. Consequently, the structural responses can also be Gaussian stochastic processes with zero-mean. To solve the structural response statistics under the stochastic excitation, a state-space representation is recommended. For the chimney with d-TMISs, the state-space description of Eq. (7) can be expressed as

$$\begin{aligned} \dot{\boldsymbol{x}}_{\mathrm{s}}(t)&=\boldsymbol{A}_{\mathrm{s}}\boldsymbol{x}_{\mathrm{s}}(t)+\boldsymbol{E}_{\mathrm{s}}\ddot{x}_{g}(t) \\ \boldsymbol{z}_{\mathrm{s}}(t)&=\boldsymbol{C}_{\mathrm{s}}\boldsymbol{x}_{\mathrm{s}}(t) \end{aligned} \tag{14}$$

where $\boldsymbol{x}_s=\begin{bmatrix} \boldsymbol{X}^{T} & \dot{\boldsymbol{X}}^{T} \end{bmatrix}^{T}$ is referred to as the state vector with respect to the nodal displacements and velocities of the chimney with d-TMISs; $\boldsymbol{z}_{\mathrm{s}}(t)$ is the response variables vector, which involves the nodal displacements of the primary chimney, the relative displacements of d-TMISs mounted on the chimney, and the absolute accelerations of the chimney with d-TMISs. In Eq. (14), the corresponding state-space matrices $\boldsymbol{A}_{\mathrm{s}}$, $\boldsymbol{E}_{\mathrm{s}}$ and $\boldsymbol{C}_{\mathrm{s}}$ can be written as

$$\boldsymbol{A}_{\mathrm{s}}=\begin{bmatrix}\mathbf{0}_{(N+2n)\times(N+2n)} & \boldsymbol{I}_{(N+2n)}\\ -\boldsymbol{M}^{-1}\boldsymbol{K} & -\boldsymbol{M}^{-1}\boldsymbol{C}\end{bmatrix}_{2(N+2n)\times 2(N+2n)},\mathbf{E}_{\mathrm{s}}=\begin{bmatrix}\mathbf{0}_{(N+2n)\times 1}\\ -\mathbf{M}^{-1}\mathbf{M}_{\mathrm{g}}\boldsymbol{\iota}\end{bmatrix}_{2(N+2n)\times 1}$$

$$\boldsymbol{C}_{\mathrm{s}}=\begin{bmatrix}\begin{bmatrix}\boldsymbol{I}_{(N)} & \mathbf{0}_{N\times 2n}\\ [\chi_1\ \ \mathbf{0}_{N\times 1}\ \ \cdots\ \ \chi_n\ \ \mathbf{0}_{N\times 1}]^{T}_{N\times 2n} & \boldsymbol{I}_{(2n)}\end{bmatrix}_{(N+2n)\times(N+2n)} & \mathbf{0}_{(N+2n)\times(N+2n)}-\boldsymbol{M}^{-1}\boldsymbol{K}-\boldsymbol{M}^{-1}\boldsymbol{C}\end{bmatrix}_{2(N+2n)\times 2(N+2n)} \tag{15}$$

Under the zero-mean white noise excitation with the PSD equal to S_0, the covariance matrix $\boldsymbol{P}$ of the state vector $\boldsymbol{x}_s$ can be calculated by the solution of the following algebraic Lyapunov equation [52]:

$$\boldsymbol{A}_{\mathrm{s}}\boldsymbol{P}+\boldsymbol{P}\boldsymbol{A}_{\mathrm{s}}^{T}+2\pi S_0\boldsymbol{E}_{\mathrm{s}}\boldsymbol{E}_{\mathrm{s}}^{T}=0 \tag{16}$$

For the output vector $z_s(t)$, which also represents the zero-mean Gaussian processes, the corresponding covariance matrix $\boldsymbol{K}_{\mathrm{z}}$ can be expressed as follows:

$$\boldsymbol{K}_{\mathrm{z}}=\boldsymbol{C}_{\mathrm{s}}\boldsymbol{P}\boldsymbol{C}_{\mathrm{s}}^{T} \tag{17}$$

Then, the variance $\sigma_{\mathrm{z},j}^2$ for the j^{th} output variable of the vector $z_{\mathrm{s}}(t)$ is obtained by the j^{th} diagonal entry of $\boldsymbol{K}_{\mathrm{z}}$, written as

$$\sigma_{z,j}^2=\boldsymbol{n}_j^{T}\boldsymbol{K}_{z}\boldsymbol{n}_j \tag{18}$$

where $\boldsymbol{n}_j$ is the column vector of zeros with a replaced one in its j^{th} element.

3. Optimal control strategy

3.1. Placement and parameters of d-TMISs

For the application of d-TMISs, it is essential to determine the placement of d-TMISs and the parameters of each TMIS employed in the multimode control of the high-rise chimney. By performing the modal analysis, the placement for each of the TMISs in the application of multimode control is determined by at which the modal shape amplitude is the largest or the larger of the specifying control mode of the uncontrolled chimney, i.e., the i^{th} TMIS adopted for the i^{th} mode control is placed at the node of the chimney model with the largest or larger modal shape amplitude of the i^{th} mode. This is done to avoid a heavy additional mass placed in a single placement where the modal shape amplitudes may be the largest for different controlled modes. The larger modal shape amplitude for determining the location of d-TMISs is also recommended here for this situation. The implication for the determination of the placement of d-TMISs is further checked in the case study illustrated in Section 4.

According to the configuration of the TMIS described above, five parameters must be obtained for the design of a TMIS. For convenience of expression, the parameters of the i^{th} TMIS are defined in a dimensionless form as follows:

$$\mu_{t,i}=\frac{m_{t,i}}{M_{eq,i}},\mu_{in,i}=\frac{m_{in,i}}{m_{t,i}},\lambda_{s,i}=\frac{\omega_{s,i}}{\omega_{t,i}},\lambda_{t,i}=\frac{\omega_{t,i}}{\omega_i},\xi_{d,i}=\frac{c_{d,i}}{2\sqrt{m_{t,i}k_{t,i}}} \tag{19}$$

where $\mu_{t,i}$, $\mu_{in,i}$, $\lambda_{s,i}$, $\lambda_{t,i}$, and $\xi_{d,i}$ are the equivalent mass ratio, inertance to tuned mass ratio, corner frequency ratio in the i^{th} TMIS, nominal natural frequency ratio, and nominal damping ratio for the i^{th} TMIS, respectively. $M_{eq,i}$ is the modal mass of the i^{th} mode of the chimney and can be calculated as follows:

$$M_{eq,i}=\boldsymbol{\varphi}_{normal,i}^{T}\boldsymbol{M}_{\mathrm{p}}\boldsymbol{\varphi}_{normal,i} \tag{20}$$

where $\boldsymbol{\varphi}_{normal,i}$ is the normalized i^{th} modal vector and is calculated by modal analysis. The normalization of $\boldsymbol{\varphi}_{normal,i}$ is established by setting its element with respect to the placement of the i^{th} TMIS being one. $\omega_{s,i}=\sqrt{k_{s,i}/m_{in,i}}$ and $\omega_{t,i}=\sqrt{k_{t,i}/m_{t,i}}$ are the nominal circular frequencies of the TVMD and i^{th} TMIS, respectively. ω_i is the i^{th} natural frequency of the uncontrolled chimney.

Assuming that the responses in the first n modes of the chimney are suppressed using d-TMISs, the number of parameters to be determined is $5n$. This can hinder the calculation for the optimal design of d-TMISs for high-rise chimneys. The extended fixed-point technique [40] is adopted in this study to simplify the optimization of d-TMISs. According to the derivation in [40], the extended fixed-point theory is determined with the single-degree-of-freedom (SDOF) structure. Hence, modal decomposition is adopted in the multimode control of a multi-degree-of-freedom chimney. Herein, each of the modal responses can be regarded as the response of an equivalent SDOF system. This aspect is reflected in the definition of the dimensionless parameter of the i^{th} TMIS in Eq. (19). Using the extended fixed-point theory, the optimum parameters $\mu_{in,i}$, $\lambda_{s,i}$, and $\lambda_{t,i}$ corresponding to the i^{th} mode control can be constrained based on $\mu_{t,i}$ as follows:

$$\mu_{in,i}=\frac{2\mu_{t,i}}{(1+2\mu_{t,i})^2},\lambda_{s,i}=1+2\mu_{t,i},\lambda_{t,i}=\sqrt{\frac{1}{(1+\mu_{t,i})(1+2\mu_{t,i})}} \tag{21}$$

In addition, the distribution pattern of $m_{t,i}$ and ξ_i are assumed to be positively correlated with the attached nodal displacements of the uncontrolled chimney. Although this assumption for the parameter distribution pattern of d-TMISs may not be the most efficient solution, it can be simple and effective. Thus, $m_{t,i}$ and ξ_i can be calculated as

$$m_{t,i}=\psi_i^{\beta}\tilde{m}_t,\xi_{d,i}=\psi_i^{\beta}\tilde{\xi}_d \tag{22}$$

where $\tilde{m}_t$ and $\tilde{\xi}_d$ are the generalized mass and nominal damping ratio that are used to determine $m_{t,i}$ and $\xi_{d,i}$, respectively; β is the parameter correlation index. In general, it is recommended that structural control devices be installed at the positions (in structures) that display large responses to ensure their efficient utilization. Hence, the parameters of d-TMISs are set to have positive correlations with the nodal displacements ($\beta\geqslant 1$). This implies that a TMIS with larger parameter values can be mounted at the location on the chimney where the seismic responses are large. A trail calculation is recommended for determining β by considering both the demand of the tuned mass and multimode control effect of the d-TMISs.ψ_i is the normalized nodal displacement of the chimney with respect to the nodal displacement and is expressed as

$$\psi_i=\frac{\sigma_{z0,i}}{\sigma_{z0,N}} \tag{23}$$

where $\sigma_{z0,N}$ and $\sigma_{z0,i}$ are the root mean square (RMS) values of the displacements of the topmost node and of the node attached to the i^{th} TMIS, respectively, in the uncontrolled chimney. These can be calculated using the root square of the zero-mean variances as described in Subsection 2.3.

For a high-rise chimney using d-TMISs, a TMIS generally needs to be mounted at the topmost node to suppress the responses in the

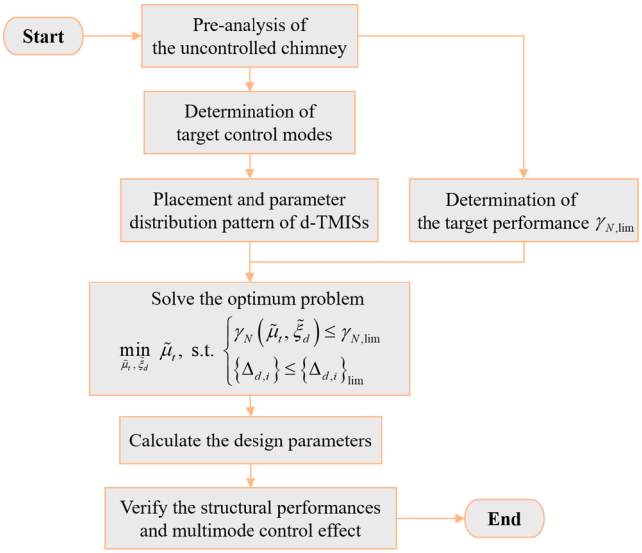

Fig. 3. Design flowchart of optimal multimode control of a chimney using d-TMISs.

fundamental mode. Therefore, according to the assumed distribution pattern of $m_{t,i}$ and ξ_i above, the calculation of $\tilde{m}_t$ and $\tilde{\xi}_d$ can be considered to be equivalent to the calculation of $m_{t,1}$ and $\xi_{d,1}$, respectively. Then, $\mu_{t,i}$ and $\xi_{d,i}$ can be obtained as follows:

$$\mu_{t,i} = \frac{\psi_i^\beta \tilde{m}_t}{M_{eq,i}} = \frac{\psi_i^\beta M_{eq,1}}{M_{eq,i}}\mu_{t,1} = \frac{\psi_i^\beta M_{eq,1}}{M_{eq,i}}\tilde{\mu}_t, \xi_{d,i} = \psi_i^\beta \xi_{d,1} = \psi_i^\beta \tilde{\xi}_d \tag{24}$$

where $\tilde{\mu}_t$ is the generalized equivalent mass ratio and is equal to $\mu_{t,1}$. Consequently, based on the above illustration, all the parameters of the additional d-TMISs can be obtained when $\tilde{\mu}_t$ and $\tilde{\xi}_d$ are determined. These two parameters are calculated with the optimization proposed below.

3.2. Optimization strategy

The optimal multimode control strategy is introduced here for the chimney using d-TMISs to obtain the corresponding design parameters. The structural performances need to be quantified appropriately to obtain the optimal design parameters of the additional d-TMISs. For a high-rise RC chimney, the curvature at a particular section or the drift response (top displacement / chimney height) is generally recommended for use as the performance index under seismic excitation [1,11]. Considering that the displacement of a chimney is closely correlated with its curvature and drift responses, the displacement response (rather than the acceleration response) is selected as the performance index in the optimization of d-TMISs. For such a cantilever structure, the top displacement of the chimney determines the structural stresses. Hence, the top displacement response performance index γ_N is defined with respect to the uncontrolled chimney for evaluating the performance of the chimney with d-TMISs, as follows:

$$\gamma_N(\mu_{t,i}, \mu_{\text{in,i}}, \lambda_{\text{s,i}}, \lambda_{\text{t,i}}, \xi_{\text{i}}) = \frac{\sigma_{z,N}}{\sigma_{z0,N}} \tag{25}$$

where $\sigma_{z,N}$ is the RMS value of the displacements of the topmost node of the chimney with d-TMISs.

In addition, considering the additional action of the tall and slender structure, a lighter mass of the added device is favorable for the structural performance. $\tilde{\mu}_t$ is selected as the evaluation indicator for the chimney with d-TMISs because the total additional tuned mass $m_{t,\text{total}} = \sum_{i=1}^{n} m_{t,i}$ of d-TMISs is correlated with $\tilde{\mu}_t$ based on the simplification mentioned above. As a tuned-type device, the stroke of the TMIS needs to be concerned considering its working space. Consequently, the relative displacement $\Delta_{d,i}$ of the i^{th} TMIS is selected as another control index for the application of d-TMISs in a high-rise RC chimney.

With the context illustrated in Subsection 3.1, the determination of parameters in the d-TMISs' optimization can be simplified as the calculation of $\tilde{\mu}_t$ and $\tilde{\xi}_d$. Therefore, the optimal multimode control design of a high-rise RC chimney can be described as a three-objective (i.e., γ_N, $\mu_{t,1}$, and $\Delta_{d,i}$) optimum problem with two design parameters (i.e., $\mu_{t,1}$ and $\xi_{d,1}$). Based on the suggestions in [53], this optimum problem is transformed into a single-objective design (SOD) using the ε-constraint approach. In SOD, $\tilde{\mu}_t$ is selected as a single objective, whereas γ_N and the relative displacement vector $\{\Delta_{d,i}\}$ with respect to the relative displacement of each TMIS are constrained by the target top displacement response performance index $\gamma_{N,lim}$ and the target relative displacement vector $\{\Delta_{d,i}\}_{lim}$. A safety redundancy coefficient α is set in the constraint condition of $\{\Delta_{d,i}\}$ to realize flexible adjustment and consider the performance redundancy of the relative displacement of the d-TMISs. α ($\alpha \leqslant 1$) can be determined by considering the trade-off between the actual working space of the d-TMISs and the demand of $\tilde{\mu}_t$. Thus, the optimization of a high-rise RC chimney using d-TMISs can be formulated as follows:

$$\min_{\tilde{\mu}_t,\tilde{\xi}_d} \tilde{\mu}_t \text{ subjected to } \begin{cases} \gamma_N\left(\tilde{\mu}_t, \tilde{\xi}_d\right) \leqslant \gamma_{N,lim}\{\Delta_{d,i}\} \leqslant \alpha\cdot\{\Delta_{d,i}\}_{lim} \\ \tilde{\mu}_{t,min} \leqslant \tilde{\mu}_t \leqslant \tilde{\mu}_{t,max} \\ \tilde{\xi}_{d,min} \leqslant \tilde{\xi}_d \leqslant \tilde{\xi}_{d,max} \end{cases} \tag{26}$$

where $\tilde{\mu}_{t,min}$ and $\tilde{\xi}_{d,min}$ represent the lower bounds of $\tilde{\mu}_t$ and $\tilde{\xi}_d$, respectively, and $\tilde{\mu}_{t,max}$ and $\tilde{\xi}_{d,max}$ represent their upper bounds.

3.3. Design flowchart

The following are the steps for the optimal multimode control design of the high-rise RC chimneys using d-TMISs according to the above illustration mentioned. A corresponding flowchart is depicted in Fig. 3.

Step 1: *Preanalysis of the uncontrolled chimney*. Conduct modal analysis to obtain the structural frequencies and modal shapes, and calculate the response statistics of the uncontrolled chimney under excitation by a zero-mean Gaussian white noise. The fundamental information of the uncontrolled chimney (e.g., the natural frequencies ω_i and mode masses $M_{eq,i}$) can be recorded.

Step 2: *Determination of the structural modes (to be controlled), placement, and parameter distribution pattern of d-TMISs, and the target performances to be achieved through optimization*. Select the target structural

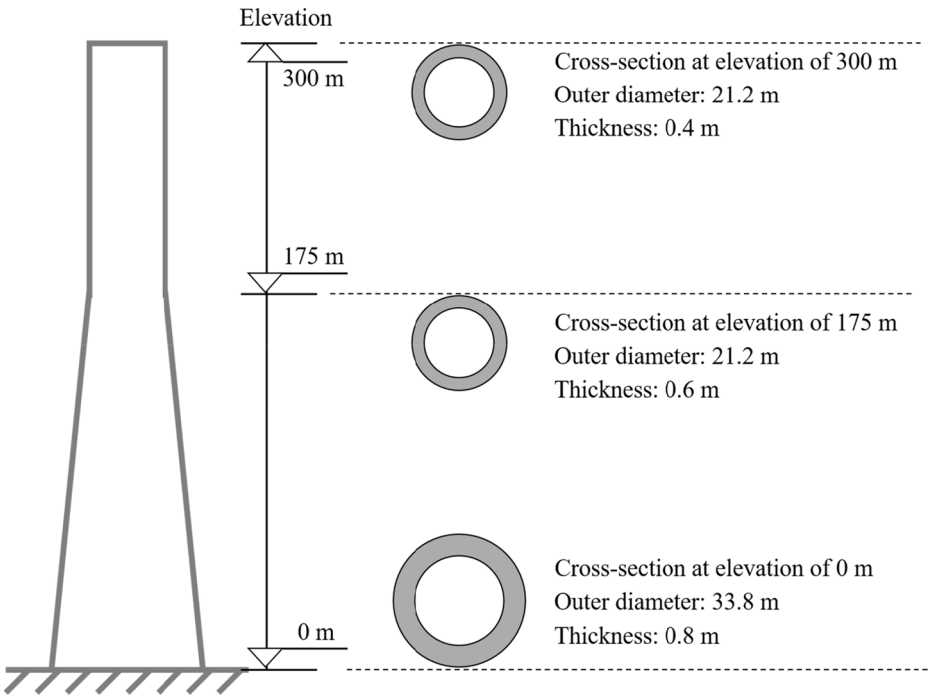

Fig. 4. Geometrical graph and dimensions at characteristic sections of the chimney.

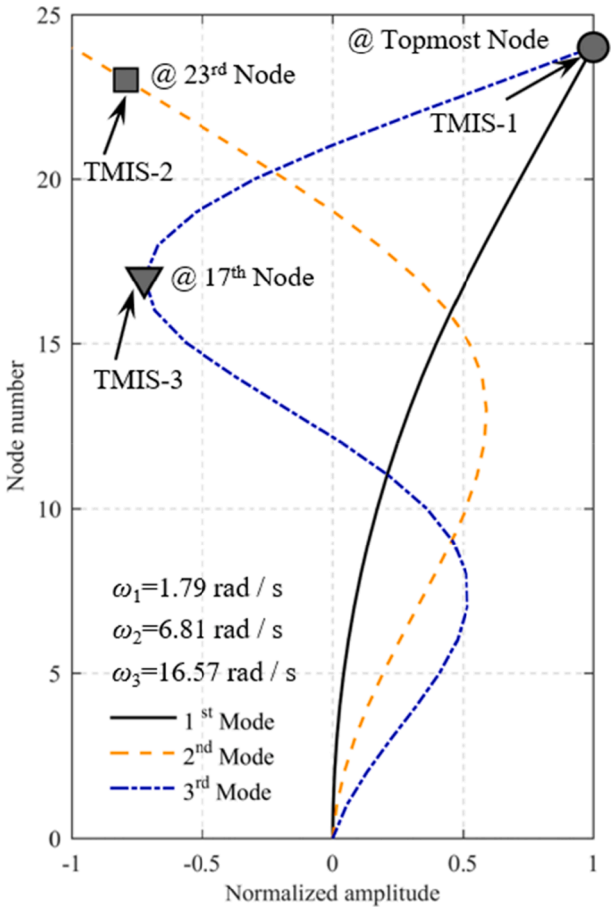

Fig. 5. Mode shapes of the uncontrolled chimney and the placement of d-TMISs.

modes to be controlled according to the modal mass participation factor Γ_i. Then, determine the placement of each TMIS based on the largest or larger amplitude of the structural mode shape. The distribution pattern of the parameters of the d-TMISs can be obtained using Eqs. (22) and (23) after the nodal response statistics of the uncontrolled chimney is calculated and the parameter correlation index β is determined by a trail calculation process. The target percentage of the total mass participation for determining the controlled modes of chimney can be 85%, based on [54,55]. The target top displacement response performance index $\gamma_{N,lim}$ can be set based on the RMS value of the topmost node of the uncontrolled chimney under external excitations and the corresponding seismic demand. It is recommended that the target relative displacement vector $\{\Delta_{d,i}\}_{lim}$ for the d-TMISs do not exceed the relative displacements of the corresponding traditional d-TMDs. The traditional d-TMDs are located at the same nodes and composed of identical tuned masses, tuning springs, and damping elements as the corresponding d-TMISs. In addition, an appropriate safety redundancy coefficient α ($\alpha \leqslant 1$) is recommended for the constraint condition of $\{\Delta_{d,i}\}$ considering the performance redundancy.

Step 3: *Solution of the optimum problem for multimode control of the chimney with d-TMISs*. Determine $\tilde{\mu}_t$ and $\tilde{\xi}_d$ by solving the SOD problem formulated as Eq. (26). The sequential quadratic programming (SQP) method can be adopted to solve this nonlinear constrained multivariable optimum problem [56].

Step 4: *Calculation of the parameters of d-TMISs*. Calculate the design parameters of the additional d-TMISs according to the distribution pattern of $\mu_{t,i}$ and $\xi_{d,i}$ defined in Eqs. (22)-(24) and the constraints of $\mu_{in,i}$, $\lambda_{s,i}$, and $\lambda_{t,i}$ expressed in Eq. (21).

Step 5: *Verification of the structural performance and multimode control effect*. Conduct time history analysis to verify the performance of the chimney with d-TMISs and a comparative analysis to examine the multimode control effect of d-TMISs designed according to the proposed multimode control optimization.

To verify the performance of the chimney with d-TMISs, the top displacement response performance index γ_N (defined in Eq. (25)) under different excitations should be compared with the target top displacement response performance index $\gamma_{N,lim}$. It is recommended that the peak

Table 1
Optimal design parameters of d-TMISs for multimode control of chimney.

TMIS number	Designed dimensionless parameters of d-TMISs				
	$\mu_{t,i}$	$\mu_{in,i}$	$\lambda_{s,i}$	$\lambda_{t,i}$	$\xi_{d,i}$
TMIS-1	0.073	0.111	1.146	0.901	0.025
TMIS-2	0.034	0.059	1.068	0.952	0.021
TMIS-3	0.008	0.016	1.016	0.988	0.007

Table 2
Practical parameters of d-TMISs.

TMIS number	Designed parameters of d-TMISs				
	$m_{t,i}$(kg)	$m_{in,i}$(kg)	$k_{t,i}$(N/m)	$k_{s,i}$(N/m)	$c_{d,i}$(N·s/m)
TMIS-1	3.135×10^5	3.485×10^4	8.231×10^5	1.202×10^5	2.540×10^4
TMIS-2	2.704×10^5	1.605×10^4	1.137×10^7	7.696×10^5	7.561×10^4
TMIS-3	8.381×10^4	1.286×10^3	2.248×10^7	3.559×10^5	1.834×10^4

response performance index $\gamma_{N,\text{peak}}$ and relative displacement performance index $\gamma_{\Delta_d,i}$ also be examined as supplementary verifications of the peak top displacement response mitigation effect and the constraint of $\{\Delta_{d,i}\} \leqslant \alpha \cdot \{\Delta_{d,i}\}_{lim}$ in the optimization of d-TMISs, respectively. These can be calculated as

$$\gamma_{N,\text{peak}} = \frac{{}_{max}d_{z,N}}{{}_{max}d_{z0,N}}, \gamma_{\Delta_d,i} = \frac{{}_{\text{TMIS}}\sigma_{\Delta_d,i}}{{}_{\text{TMD}}\sigma_{\Delta_d,i}} \tag{27}$$

where ${}_{max}d_{z,N}$ and ${}_{max}d_{z0,N}$ are the maximum top displacements of the chimney with d-TMISs and the uncontrolled chimney, respectively. ${}_{TMIS}\sigma_{\Delta_d,i}$ and ${}_{TMD}\sigma_{\Delta_d,i}$ are the RMS values of the relative displacement of the i^{th} TMIS in d-TMISs and i^{th} TMD in d-TMDs, respectively.

It is recommended that eigenvalue analyses be first conducted to obtain the natural frequencies of the uncontrolled chimney and the chimney with d-TMISs for a preliminary evaluation of the tuning effect of the d-TMISs for multimode control. The installation of the d-TMISs on the chimney provides an additional degree of freedom, whereby the frequency characteristic of the chimney is altered. In general, the frequency of the target mode is split and varied around the original frequency of the chimney. Otherwise, the design parameters of d-TMIS should be revised. Furthermore, it is recommended that the frequency response functions (FRFs) of the responses of the chimney with different d-TMISs be drawn for different target mode control and that these be compared to verify the expected multimode control effect.

4. Illustrative case study

4.1. Multimode control design

4.1.1. Model information

A benchmark model of a 300 m high-rise RC chimney from the research of Liang et al. [57] is adopted here as an illustrative case to examine the proposed method for optimal multimode control using d-TMISs. The geometrical graph and characteristic sizes of the chimney are shown in Fig. 4. There is an abrupt variation in the geometry at an elevation of 175 m of the RC chimney. From the base to this elevation, the outer diameter of the chimney decreases gradually from 33.8 m to 21.2 m along the height. Above this elevation, the chimney has a uniform cross-section with an outer diameter of 21.2 m. The elastic modulus and density of the concrete are considered to be 2.5×10^{10}N/m^2 and 2400 kg/m^3, respectively. This chimney is divided into 24 equivalent beam elements each with a height of 12.5 m. In addition, for simplification, the cross-section of each beam element is assumed to be uniform throughout its height. Only one translational direction of the chimney is investigated considering its symmetry. The chimney employed herein is located in a 2 GW power plant in Hubei province, China. Considering the possibility of the potential construction site, the rigid foundation is adopted in the chimney model according to the Chinese code for seismic deign [58]. Referring to Subsection 2.1, the numerical model of the RC chimney is established with a 24-DOF system. The inherent damping matrix of the chimney is expressed by assuming a constant damping ratio of 0.05 for all the modes according to the recommendation of the CICIND code [1] and Chinese code for design of chimneys [59]. The total mass of the chimney $M_{total} = \sum_{k=1}^{N} m_k$ is calculated to be 3.326×10^7 kg.

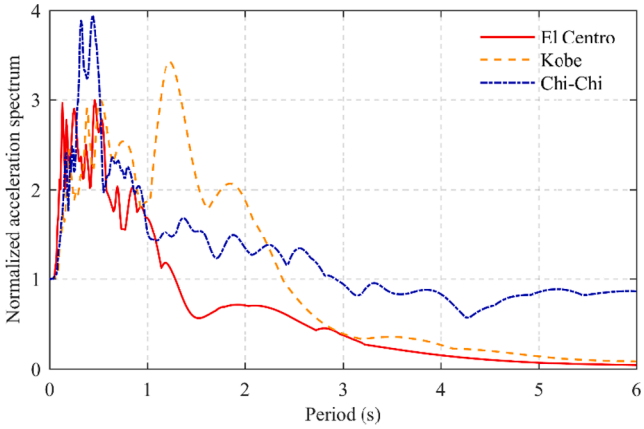

Fig. 6. Acceleration response spectra of natural seismic waves.

Modal analysis is conducted for the high-rise RC chimney. According to the analysis results, the modal mass participation factors Γ_i of the first three modes ($\Gamma_1 = 0.48$, $\Gamma_2 = 0.26$, and $\Gamma_3 = 0.13$) are relatively large compared with those of the other modes. Moreover, the sum of Γ_i for the first three modes is larger than 0.85. Hence, the first three modes of the chimney are selected to be controlled. The natural vibration frequencies ω_i of the first, second, and third modes are 1.79 rad/s, 6.81 rad/s, and 16.57 rad/s, respectively. The normalized mode shapes (with one as their largest amplitude) for the first three modes are depicted in Fig. 5. Then, the locations of the three TMISs (d-TMISs) are determined as follows: TMIS-1 for the first mode at the 24th node (i.e., the topmost node), TMIS-2 for the second mode at the 23rd node (height of 287.5 m of the chimney), and TMIS-3 for the third mode at the 17th node (height of 212.5 m of the chimney). In addition, the modal masses $M_{eq,i}$ for the first, second, and third modes are calculated using Eq. (20) and are obtained as 4.295×10^6 kg, 7.991×10^6 kg, and 1.058×10^7 kg, respectively.

4.1.2. Solution of the d-TMIS parameters

To suppress the vibration of the RC chimney, the target top displacement response performance index $\gamma_{N,lim}$ is set to 0.7 according to the preanalysis results of the uncontrolled chimney under external excitations and considering the seismic demand. In Section 3.1, it is recommended that the parameters of the d-TMISs be positively correlated with the nodal displacements of the chimney (i.e., $\beta \geqslant 1$). To determine β in the optimization of d-TMISs, a trial calculation is conducted with the values of β from one to five. The results show that the demand value of $\tilde{\mu}_t$ under a $\gamma_{N,lim}$ of 0.7 decreases with the increase in β. Furthermore, the peak value of the frequency response function for the third mode of the chimney using d-TMISs increases with the increase in β. This indicates that a large β is favorable for reducing the demand of $\tilde{\mu}_t$ under a certain $\gamma_{N,lim}$. This is mainly owing to the predominant contribution of the fundamental mode to the structural responses. However, β cannot be too large considering the high mode control effect of the high-rise chimney. If it is, the parameters of the additional TMISs would be concentrated on

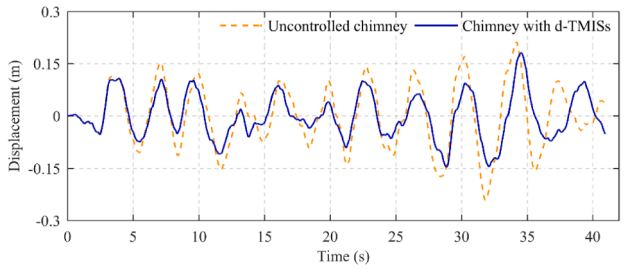

(a) White noise (γ_N=0.71 , $\gamma_{N,\,peak}$=0.75)

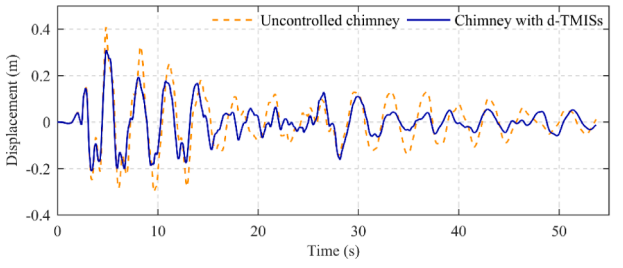

(b) El Centro (γ_N=0.74 , $\gamma_{N,\,peak}$=0.76)

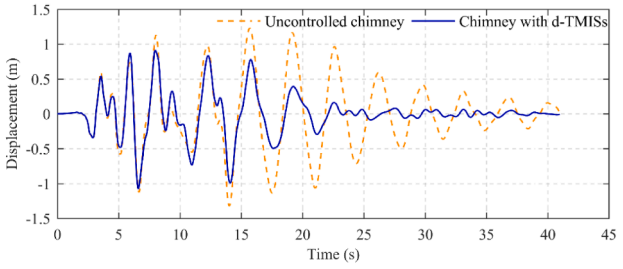

(c) Kobe (γ_N=0.65 , $\gamma_{N,\,peak}$=0.81)

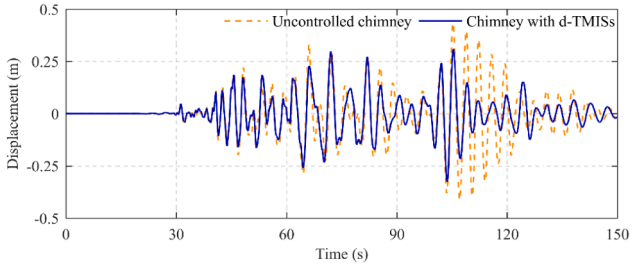

(d) Chi-Chi, (γ_N=0.72 , $\gamma_{N,\,peak}$=0.75)

Fig. 7. Top displacement responses of the uncontrolled chimney and the chimney with d-TMISs.

TMIS-1, which is installed on the topmost node for the first mode control. Consequently, $\beta = 2$ is adopted in the optimization of the d-TMISs according to the results of the trial calculation using values of β from one to five and considering the balance between the demand of the tuned mass and multimode control effect. As a constraint condition in the optimization of the d-TMISs, their target relative displacements (which are expressed as the vector $\{\Delta_{d,i}\}_{lim}$) are determined to be equal to the relative displacements of the d-TMDs that are placed at the same locations and equipped with identical tuned masses, tuning springs, and damping elements as the corresponding d-TMISs. In addition, a safety redundancy coefficient α is considered in the constraint condition of $\{\Delta_{d,i}\}$ to realize a flexible adjustment and take into account the performance redundancy of the relative displacement of the d-TMISs. For the convenience of calculation, the following is considered to be the constraint with respect to $\{\Delta_{d,i}\}$ in the optimization of the d-TMISs: the ratio of the corresponding entry in $\{\Delta_{d,i}\}$ to that in $\{\Delta_{d,i}\}_{lim}$ is smaller than α. In this study, α is set as one considering the practical installation space of the d-TMISs and the corresponding analysis results presented below. The lower bounds of $\tilde{\mu}_t$ and $\tilde{\xi}_d$ are set as 10^{-4} and 10^{-3}, respectively, and their upper bounds are set as 1 and 0.9, respectively, in the d-TMISs optimization.

$\tilde{\mu}_t$ and $\tilde{\xi}_d$ are determined to be 0.073 and 0.025, respectively, by solving the optimum problem expressed in Eq. (26). Then, the parameters of d-TMISs for multimode control of the chimney can be obtained according to Eqs. (21) and (24), and are listed in Table 1. The practical parameters of the d-TMISs are also listed in Table 2 for a further understanding of the actual characteristic of the proposed device.

4.1.3. Time history analysis

Time history analysis is performed herein to verify the performance of the chimney with the designed d-TMISs. Three natural seismic waves and a white noise excitation with zero mean are adopted to conduct this analysis. The three typical seismic records include the El Centro record (1940, PGA = 0.28 g), Kobe record (1995, PGA = 0.62 g), and Chi-Chi record (1999, PGA = 0.13 g). These are selected from the strong ground motion database of the Pacific Earthquake Engineering Research Center (PEER) [60,61]. Fig. 6 shows the normalized acceleration response spectra of these three seismic waves.

The time history displacement responses of the topmost nodes for both uncontrolled chimney and chimney with designed d-TMISs under different dynamic excitations are depicted in Fig. 7. Both RMS response performance index γ_N and peak response performance index $\gamma_{N,\text{peak}}$ of the top displacements are recorded to assess the response reduction effect of the d-TMISs in the high-rise chimney. γ_N and $\gamma_{N,\text{peak}}$ can be calculated using Eqs. (25) and (27), respectively.

The results in Fig. 7 show that the use of the designed d-TMISs in the chimney effectively mitigated both peak responses and RMS values of the top displacements. Although the reduction in peak displacements is not as good as that in the RMS values of the top displacement under different excitations, these can be considered acceptable. In addition, the response performance indices γ_N of the RMS value of the top displacements are close to the target value of $\gamma_{N,lim} = 0.7$ under both white noise and seismic excitations. Hence, it is verified that the expected target seismic response reduction can be achieved by applying the proposed optimal design method using d-TMISs.

For the constraint $\{\Delta_{d,i}\} \leqslant \alpha \cdot \{\Delta_{d,i}\}_{lim}$ in the optimization, the d-TMDs are recommended to be used as references for the d-TMISs. To evaluate the constraint $\{\Delta_{d,i}\} \leqslant \alpha \cdot \{\Delta_{d,i}\}_{lim}$ in the optimization of the d-TMISs, the relative displacement reduction ratio $\gamma_{\Delta_{d,i}}$ of the d-TMDs and d-TMISs is recommended to be used. It can be calculated using Eq. (27). Note that in the definition of $\gamma_{\Delta_{d,i}}$, the i^{th} TMD in d-TMDs has the same location and is equipped with identical tuned mass, tuning spring, and damping element as the i^{th} TMIS in d-TMISs. The dynamic responses of the relative displacements of each TMIS and TMD and the corresponding $\gamma_{\Delta_{d,i}}$ under the white noise excitation are shown in Fig. 8. It is evident that the relative displacement response for each TMIS is less than that of the corresponding TMD and that all the ratios $\gamma_{\Delta_{d,i}}$ are less than one. In addition, the difference in vibration characteristics are evident from the relative displacement responses of the different TMISs and TMDs used for the specified mode control of the chimney. The relative displacement responses of TMIS-1 and TMD-1 for the first-mode control of the chimney exhibit low-frequency vibration characteristics. Meanwhile, middle- and high-frequency vibration characteristics are respectively observed for TMIS-2 and TMD-2 in the second-mode control, and for TMIS-3 and TMD-3 in the third-mode control of the chimney. These phenomena reveal the tuned effect of the devices used for the specified mode control. All the ratios $\gamma_{\Delta_{d,i}}$ under different seismic excitations are also listed in Table 3. These values are less than one. It is demonstrated the constraint $\{\Delta_{d,i}\} \leqslant \alpha \cdot \{\Delta_{d,i}\}_{lim}$ is satisfied in the optimization of the d-TMISs.

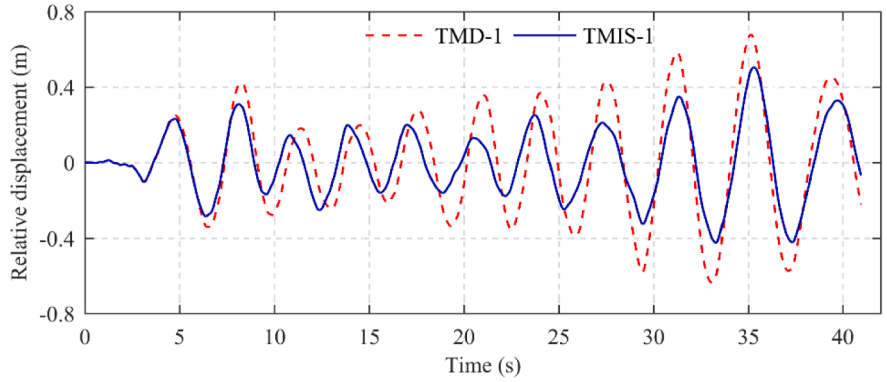

(a) Relative displacements of TMD-1 and TMIS-1, $\gamma_{\Delta_d,1}$=0.67

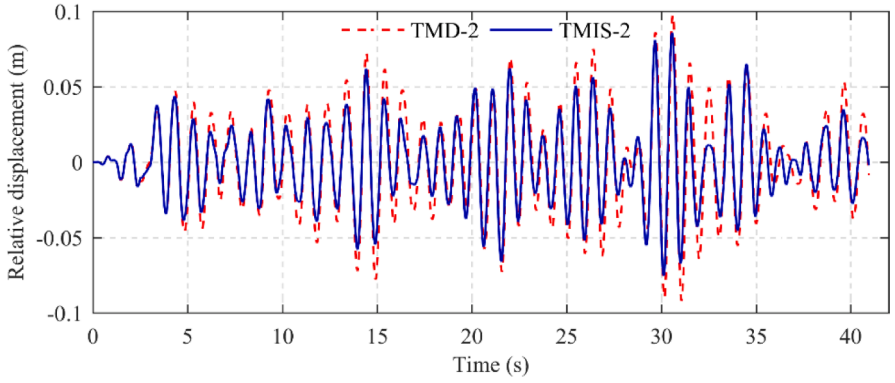

(b) Relative displacements of TMD-2 and TMIS-2, $\gamma_{\Delta_d,1}$=0.80

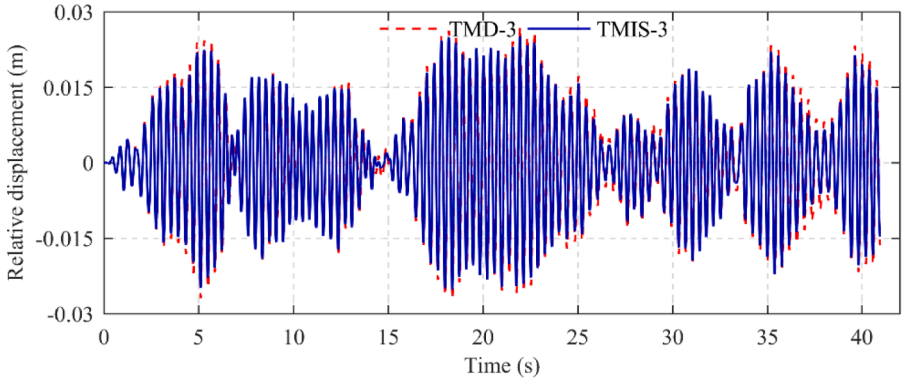

(c) Relative displacements of TMD-3 and TMIS-3, $\gamma_{\Delta_d,3}$=0.96

Fig. 8. Relative displacements of the d-TMDs and d-TMISs used in the chimneys (white noise excitation).

Table 3
Relative displacement ratios of the d-TMDs to d-TMISs used in the chimneys.

Earthquake excitation	Relative displacement ratio		
	$\gamma_{\Delta_d,1}$	$\gamma_{\Delta_d,2}$	$\gamma_{\Delta_d,3}$
El Centro	0.73	0.82	0.94
Kobe	0.60	0.84	0.95
Chi-Chi	0.66	0.85	0.97

4.1.4. *Effectiveness of d-TMISs for multimode control*

Eigenvalue analyses are first conducted for both the uncontrolled chimney and the chimney with the designed d-TMISs to explain the tuning effect of the d-TMISs for multimode control. The mass matrix $\boldsymbol{M}$and stiffness matrix $\boldsymbol{K}$ of the chimney with d-TMISs can be obtained by using Eqs. (8) and (10) and the parameters of the d-TMISs in Table 2 for the eigenvalue analysis. The natural circular frequencies of these two structures are compared in Table 4. It is evident that an additional TMIS

Table 4
Natural circular frequencies of the uncontrolled chimney and the chimney with d-TMISs.

Uncontrolled chimney		Chimney with d-TMISs	
Mode number	Circular frequency	Mode number	Circular frequency
1	1.79	1	1.38
		2	1.74
		3	2.18
2	6.81	4	5.82
		5	6.78
		6	7.96
3	16.57	7	15.32
		8	16.58
		9	17.86
4	28.55	10	28.59
5	42.97	11	42.98

used to control a specified mode of the chimney can add two degrees of freedom. Consequently, when the d-TMISs are adopted to control the first three modes of the chimney, these modes are split into three pairs of modes. Each pair is composed of three modes with close frequencies. In addition, the middle frequency in a pair is close to the original frequency of the uncontrolled chimney, and the other two frequencies are separated beside the original frequency. Nevertheless, the frequencies with respect to the uncontrolled modes of the chimney with d-TMISs (10th and 11th modes) are almost unaltered compared with those for the corresponding modes of the uncontrolled chimney (4th and 5th modes). This regularity can also be observed for other higher modes of the uncontrolled chimney and the chimney with d-TMISs that are not listed in Table 4. It is noteworthy that the middle frequency in a pair of modes of the chimney with d-TMISs differs more from the corresponding frequency of the uncontrolled chimney for the first mode compared with that for the higher modes (Table 4). This is mainly because the largest tuned mass is equipped for the first mode control and the smaller tuned mass is set for the higher mode, considering the corresponding modal mass participation factor. To summarize, the target modes of the chimney can be tuned accurately using the d-TMISs designed by the optimal method proposed above.

To provide further insight into the multimode control of the chimney using d-TMISs, the proposed optimal design method is adopted also for single-mode and two-mode control using a single TMIS (s-TMIS, placed at the topmost node) and two distributed TMISs (2d-TMISs, placed at the topmost and 23rd nodes), respectively, under identical target performances (i.e., $\gamma_N \leqslant 0.7$ and $\{\Delta_{d,i}\} \leqslant \{\Delta_{d,i}\}_{lim}$). The d-TMISs used to control the first three modes of the chimney are renamed as 3d-TMISs for the convenience of differentiation. The frequency response functions (FRFs) of the top displacements and accelerations for the uncontrolled chimney and the chimney controlled in different modes (i.e., the chimney with s-TMIS, 2d-TMISs, and 3d-TMISs) are shown in Fig. 9. The FRF $H(\Omega)$ can be calculated as follows:

$$H(\Omega) = \boldsymbol{n}_j^T \boldsymbol{C}_s \left[\mathrm{i}\Omega \boldsymbol{I}_{(N+2n)} - \boldsymbol{A}_s \right]^{-1} \boldsymbol{E}_s \tag{28}$$

where i is the imaginary unit and Ω denotes the frequency of the external excitation. To illustrate quantitatively, the peak values for the first three modes for the FRFs of the uncontrolled chimney and the chimney with 3d-TMISs are presented in Fig. 9. In FRFs, the resonant peaks of the top displacement and acceleration in the uncontrolled chimney are split and reduced upon the installation of TMISs for the structural control of different modes. Moreover, for each designed case shown in Fig. 9, only the peaks of the displacement and acceleration for the target modes are decreased, whereas the peaks of the displacement and acceleration for the other irrelevant modes are almost unaltered. The proposed optimal multimode design can be considered to be effective for structural response control involving the target modes without influencing the irrelevant modes.

Fig. 9a shows that the resonant peaks of the top displacement are reduced for the first two modes significantly, whereas the reduction effect in the third mode is not as good as that of the first two modes for the chimney using 3d-TMISs. This is mainly because the parameters of TMIS-3 that are set to controll the third mode of the chimney may be a little small under the assumed parameter distribution pattern. However, considering the performance redundancy and the reduction effect of the resonant peak of the top acceleration for the third mode shown in Fig. 9b, it is recommended that the response involving the third mode of chimney to be controlled using TMIS-3. Furthermore, to achieve a better target mode control effect, the parameter distribution pattern of d-TMIS expressed in Eqs. (22)–(24) can be modified, or the parameters of TMIS that do not perform as anticipated can be adjusted individually under the condition of target top displacement response reduction. It is noteworthy that to obtain a better high-mode control by altering the parameters of the d-TMISs, a large additional tuned mass of d-TMISs can be required and a balance between the cost and high-mode control effect should be considered.

4.2. Improvement of d-TMISs

In this section, the traditional d-TMDs are adopted for the high-rise

Table 5
Parameters in the design cases and the corresponding tuned mass reduction ratios.

Case ID	Design of d-TMDs		Design of d-TMISs			α_T
	$\tilde{\mu}_t$	γ_N	$\gamma_{N,lim}$	$\tilde{\mu}_t$	$\tilde{\xi}_d$	
Case-A	0.02	0.83	0.83	0.015	0.003	25%
Case-B	0.04	0.78	0.78	0.027	0.006	33%
Case-C	0.06	0.75	0.75	0.039	0.011	35%

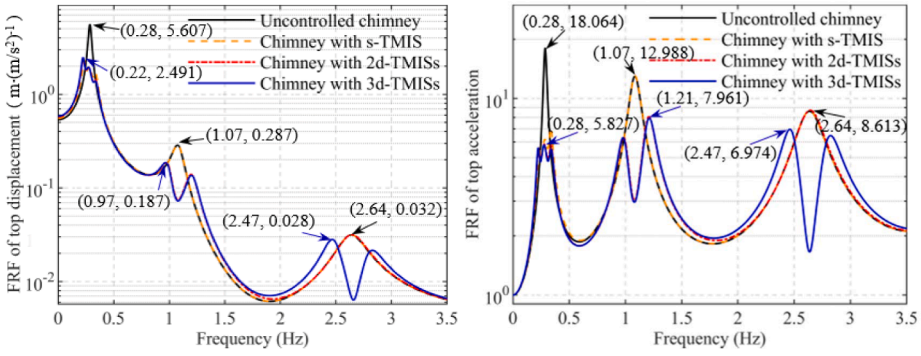

(a) Top displacement (b) Top acceleration

Fig. 9. FRFs of the uncontrolled chimney and the chimneys controlled in different modes.

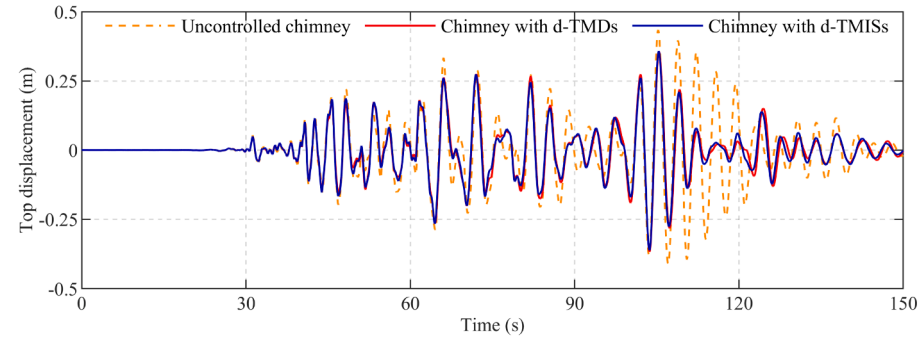

(a) Top displacement responses, $\gamma_{N,TMD} = 76\%$, $\gamma_{N,TMIS} = 75\%$

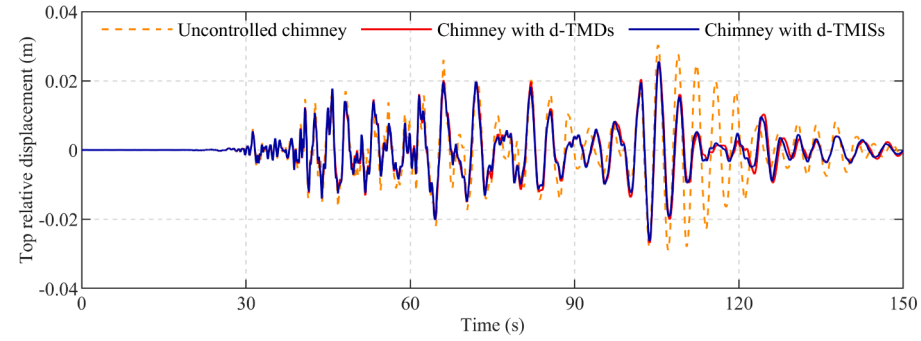

(b) Relative deflections between topmost and second to last nodes, $\gamma_{R,TMD} = 78\%$, $\gamma_{R,TMIS} = 76\%$

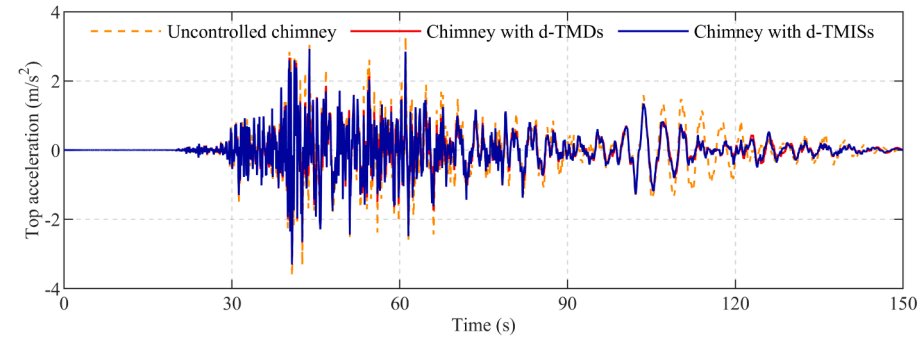

(c) Top acceleration responses, $\gamma_{A,TMD} = 83\%$, $\gamma_{A,TMIS} = 82\%$

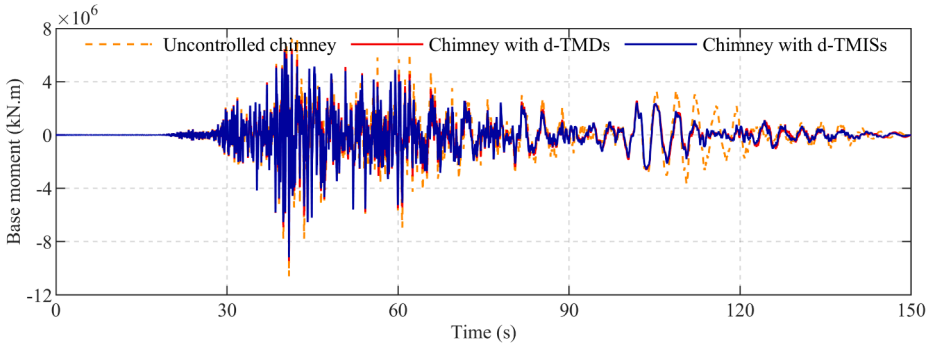

(d) Base moment responses, $\gamma_{M,TMD} = 82\%$, $\gamma_{M,TMIS} = 81\%$

Fig. 10. Seismic mitigation effect of chimney with d-TMISs and that with d-TMDs, under Chi-Chi wave.

chimney. Furthermore, the first three modes are controlled to perform a comparative study with the d-TMISs. Assuming that the installation location and parameter distribution pattern are identical to those of the d-TMISs, the d-TMDs are designed for several different generalized mass ratios $\tilde{\mu}_t$. Furthermore, Den Hartog's fixed-point theory [62] is employed to obtain the other parameters of each TMD for each of the equivalent SDOF systems of the chimney corresponding to the relevant target modes. Using the d-TMDs, three design cases (recorded as Case-A, Case-B, and Case-C) are set for $\tilde{\mu}_t$ equal to 0.02, 0.04, and 0.06, respectively. Accordingly, the top displacement response performance indices γ_N of the d-TMDs are calculated as listed in Table 5. Then, the d-TMISs are also designed using the optimal design method proposed in this study to achieve the γ_N obtained using d-TMDs. To provide an evaluation index of the lightweight effect of the d-TMISs in comparison with the traditional

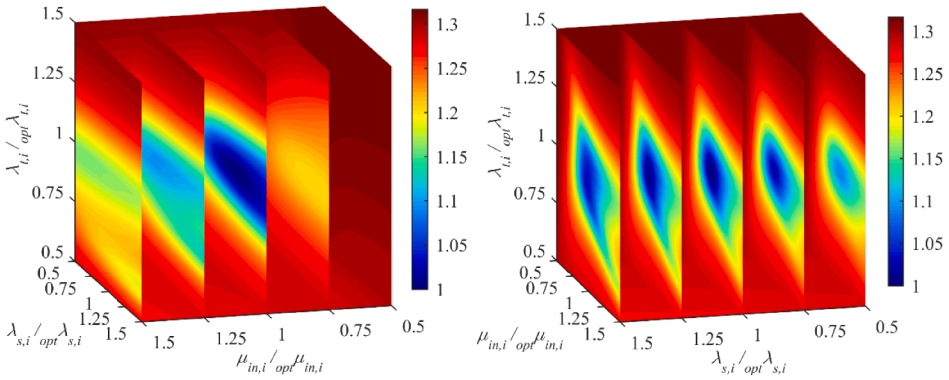

(a) Slices at constant values of $\mu_{in,i}/_{opt}\mu_{in,i}$ (b) Slices at constant values of $\lambda_{s,i}/_{opt}\lambda_{s,i}$

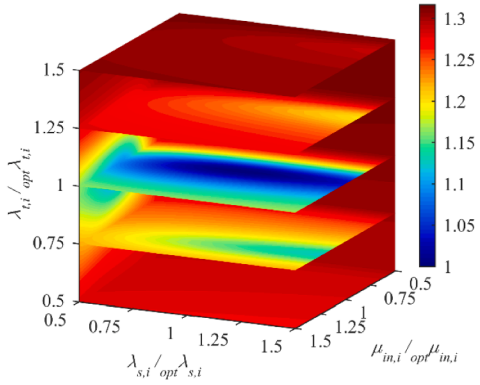

(c) Slices at constant values of $\lambda_{t,i}/_{opt}\lambda_{t,i}$

Fig. 11. Sensitivity responses of γ_N owing to the variations in $\mu_{in,i}$, $\lambda_{s,i}$ and $\lambda_{t,i}$

d-TMDs, the tuned mass reduction ratio α_T is defined as

$$\alpha_T = \frac{\tilde{\mu}_{t,TMD} - \tilde{\mu}_{t,TMIS}}{\tilde{\mu}_{t,TMD}} \times 100\% \tag{29}$$

where $\tilde{\mu}_{t,TMD}$ and $\tilde{\mu}_{t,TMIS}$ denote the generalized tuned mass ratios of the d-TMDs and d-TMISs, respectively.

The optimal design parameters of d-TMISs and the results of α_T are presented in Table 5 for each of the design cases. The tuned mass reduction ratio in these design cases is at least 25%. This indicates an apparent lightweight effect of the d-TMISs compared to the traditional d-TMDs for the multimode control of chimneys. In the TMIS, the inerter provides an additional degree of freedom and replaces part of the role of the tuned mass with a negligible gravitational mass owing to its apparent mass effect. Under an identical target top displacement response performance index, the demand of the tuned mass of the d-TMISs for seismic mitigation of the chimney is less than that for the d-TMDs.

To comprehensively evaluate the seismic responses of the chimney using d-TMISs and further compare the seismic mitigation effect of the d-TMISs with that of the d-TMDs, the top displacement, relative deflection between the topmost and second to last nodes, the top acceleration, and the base moment responses for the chimney using d-TMISs and that using d-TMDs are examined herein for Case C. Considering the limitation of article length, the corresponding seismic responses are drawn only under the Chi-Chi earthquake excitation in Fig. 10. For the convenience of quantitative analysis, the top relative deflection reduction ratio γ_R, top acceleration reduction ratio γ_A, and base moment reduction ratioγ_M are defined as follows:

$$\gamma_R = \frac{\sigma_{rd,N}}{\sigma_{rd0,N}}, \gamma_A = \frac{\sigma_{a,N}}{\sigma_{a0,N}}, \gamma_M = \frac{\sigma_{m,N}}{\sigma_{m0,N}} \tag{30}$$

where $\sigma_{rd,N}$, $\sigma_{a,N}$, and $\sigma_{m,N}$ are the RMSs of the relative deflection between the topmost and second to last nodes, the top acceleration, and the base moment responses, respectively, of the chimney with d-TMISs or d-TMDs, respectively. $\sigma_{rd0,N}$, $\sigma_{a0,N}$, and $\sigma_{m0,N}$ are the RMSs of the relative deflection between the topmost and second to last nodes, the top acceleration, and the base moment responses, respectively, of the uncontrolled chimney. Additional subscripts of TMIS and TMD are also adopted in γ_R, γ_A, and γ_M (as shown in Fig. 10) to distinguish the seismic mitigation effect of d-TMISs from that of d-TMDs.

In Case C, the d-TMDs and d-TMISs used in the RC chimney are designed to achieve an identical target top displacement performance ratio $\gamma_{N,lim}$ of 75%. Fig. 10a shows that the top displacement responses are mitigated in the time-domain as anticipated for the chimney using d-TMDs and that using d-TMISs. In addition, the relative deflections between the topmost and second to last nodes, the top accelerations, and the base moment responses are effectively reduced for the chimney using d-TMDs and that using d-TMISs (Fig. 10b–10c). Similar seismic mitigation effects are obtained for the other responses of the chimney using d-TMDs and that using d-TMISs, under an identical $\gamma_{N,lim}$. Note that the tuned mass of the d-TMISs is 35% less than that of the d-TMDs in Case C. In Fig. 10, the top relative deflection reduction ratios of the chimney using d-TMDs and those of the chimney using d-TMISs are close to the top displacement reduction ratios, whereas the top acceleration reduction ratio and base moment reduction ratio are less than the top displacement reduction ratio. This indicates that under an identical $\gamma_{N,lim}$ for the chimney using d-TMDs and that using d-TMISs, the seismic mitigation effect of the top relative deflection is close to that of the top

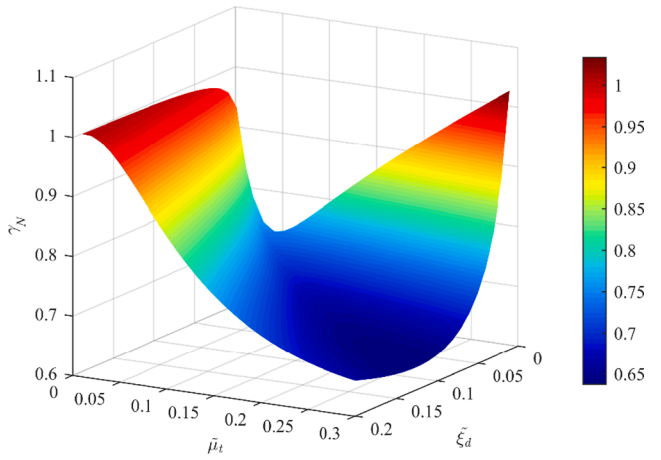

Fig. 12. Results of γ_N under different values of $\tilde{\mu}_t$ and $\tilde{\xi}_d$

displacement, whereas the seismic mitigation effects of the top acceleration and base moment are weaker than that of the top displacement.

To summarize, the d-TMISs can be considered as a lightweight vibration device used for multimode control of the seismic response of high-rise RC chimneys. With a suitable design, the dynamic responses of the chimney can be reduced comprehensively by using d-TMISs. Furthermore, the seismic response mitigation effect of the chimney with d-TMISs can be as good as that with the traditional d-TMDs under a lighter weight.

5. Parametric study

5.1. Rationality concerning the simplification and sensitivity analysis

The extended fixed-point theory is employed in Section 3.1 to determine $\mu_{in,i}$, $\lambda_{s,i}$ and $\lambda_{t,i}$ for each TMIS. Then, the optimal multimode control problem is simplified based on the assumed parameter distribution pattern of d-TMISs to just obtain the solutions for $\tilde{\mu}_t$ and $\tilde{\xi}_d$. To examine whether the application of the extended fixed-point theory is rational for the optimization of the d-TMISs, the performance of the chimney is investigated by shifting $\mu_{in,i}$, $\lambda_{s,i}$, and $\lambda_{t,i}$ away from their optimal values (${}_{opt}\mu_{in,i}$, ${}_{opt}\lambda_{s,i}$, and ${}_{opt}\lambda_{t,i}$) within a 50% range for all the equipped TMISs (Case-B is analyzed as an example). Note that the optimal inertance to tuned mass ratio ${}_{opt}\mu_{in,i}$, optimal corner frequency ratio ${}_{opt}\lambda_{s,i}$, and optimal nominal natural frequency ratio ${}_{opt}\lambda_{t,i}$ are calculated using the proposed multimode control optimization. To express the shifting of these parameter away from their optimal values with a 50% range, the ratios of the shifted parameters ($\mu_{in,i}$, $\lambda_{s,i}$, and $\lambda_{t,i}$) to those of the optimal values (${}_{opt}\mu_{in,i}$, ${}_{opt}\lambda_{s,i}$, and ${}_{opt}\lambda_{t,i}$) are defined as $\mu_{in,i}/\ {}_{opt}\mu_{in,i}$, $\lambda_{s,i}/\ {}_{opt}\lambda_{s,i}$, and $\lambda_{t,i}/\ {}_{opt}\lambda_{t,i}$, respectively, with a range of 0.5–1.5. These have been drawn on the axes of the three-dimensional diagram in Fig. 11. Then, the values of the top displacement response performance index γ_N are calculated for all the feasible possible parameter combinations in the range defined above by setting a constant combination of $\tilde{\mu}_t$ and $\tilde{\xi}_d$ calculated in Case-B. To evaluate the shifting of γ_N with the variation in the parameters of d-TMIS, the ratio $\gamma_N/\gamma_{N,original}$ of the chimney is defined and calculated for $\mu_{in,i}/\ {}_{opt}\mu_{in,i}$, $\lambda_{s,i}/\ {}_{opt}\lambda_{s,i}$, and $\lambda_{t,i}/\ {}_{opt}\lambda_{t,i}$ in the range 0.5–1.5, as shown in Fig. 11. Here, $\gamma_{N,original}$ denotes the original top displacement response performance index for the chimney with d-TMISs calculated in Case-B. In Fig. 11, $\gamma_N/\gamma_{N,original}$ is represented by the color of each point in the dyed parametric space under different combinations of $\mu_{in,i}/\ {}_{opt}\mu_{in,i}$, $\lambda_{s,i}/\ {}_{opt}\lambda_{s,i}$, and $\lambda_{t,i}/\ {}_{opt}\lambda_{t,i}$.

Fig. 11 shows that all the values of $\gamma_N/\gamma_{N,original}$ are approximately at least one as $\mu_{in,i}$, $\lambda_{s,i}$, and $\lambda_{t,i}$ vary. Hence, the determination of $\mu_{in,i}$, $\lambda_{s,i}$, and $\lambda_{t,i}$ based on the extended fixed-point theory can be considered as the optimal result for a certain combination of $\tilde{\mu}_t$ and $\tilde{\xi}_d$ solved under a preset target performance. That is, the application of the extended fixed-point theory is rational to simplify the determination of the parameters for the optimization in d-TMISs. In addition, it is observed that the color maps for the slices at constant values of $\lambda_{s,i}/\ {}_{opt}\lambda_{s,i}$ exhibit similar characteristics, whereas those for the slices at constant values of $\mu_{in,i}/\ {}_{opt}\mu_{in,i}$ and of $\lambda_{t,i}/\ {}_{opt}\lambda_{t,i}$ differ significantly. These indicate that the performance of the chimney with d-TMISs is sensitive to the variations in $\mu_{in,i}$ and $\lambda_{t,i}$, and is marginally sensitive to that in $\lambda_{s,i}$. The best seismic mitigation effect is achieved for the values of $\mu_{in,i}/\ {}_{opt}\mu_{in,i}$, $\lambda_{s,i}/\ {}_{opt}\lambda_{s,i}$, and $\lambda_{t,i}/\ {}_{opt}\lambda_{t,i}$ close to one. For the slices at constant values of $\mu_{in,i}/\ {}_{opt}\mu_{in,i}$ (Fig. 11a), the areas of cool color in the slices of $\mu_{in,i}/\ {}_{opt}\mu_{in,i}$ larger than one are larger than those in the slices of $\mu_{in,i}/\ {}_{opt}\mu_{in,i}$ smaller than one. This indicates that the values of $\mu_{in,i}/\ {}_{opt}\mu_{in,i}$ larger than one can be favorable to the seismic control of the chimney compared with those smaller than one, for certain specified sets of other parameters. In a similar analysis, this property is observed to be the converse of that of $\lambda_{t,i}/\ {}_{opt}\lambda_{t,i}$.

5.2. Parametric analysis of $\tilde{\mu}_t$ and $\tilde{\xi}_d$

The parameters $\mu_{in,i}$, $\lambda_{s,i}$, and $\lambda_{t,i}$ of the d-TMISs calculated using the extended fixed-point theory have been demonstrated above to be reasonable after $\tilde{\mu}_t$ and $\tilde{\xi}_d$ are determined. In this part, parametric analysis is conducted to investigate the performance of the chimney with d-TMISs, as shown in Fig. 12. Here, $\tilde{\mu}_t$ and $\tilde{\xi}_d$ range from 0.01 to 0.3 and 0.01–0.2, respectively. $\mu_{in,i}$, $\lambda_{s,i}$, and $\lambda_{t,i}$ are determined using Eq. (21), and γ_N is calculated using Eq. (25).

It is evident that for a low damping parameter $\tilde{\xi}_d$, γ_N first decreases and then increases with the increase in $\tilde{\mu}_t$. Hence, there is a local optimal solution for a middle $\tilde{\mu}_t$ and relatively low damping parameter $\tilde{\xi}_d$. For a high damping parameter $\tilde{\xi}_d$, γ_N decreases continuously with the increase in $\tilde{\mu}_t$, whereas the rate of increase is evidently smaller for a large $\tilde{\mu}_t$. That implies that for a large $\tilde{\mu}_t$, γ_N is not sensitive to the variation in $\tilde{\mu}_t$. It is not necessary to pursue the minimum γ_N with a significantly large $\tilde{\mu}_t$ considering the cost. For a performance-based design, there should be a balance between the values of $\tilde{\mu}_t$ and γ_N.

6. Conclusion

This study proposes the installation of ungrounded d-TMISs on high-rise chimneys for multimode control of seismic response. A corresponding optimization design method is developed for reducing the seismic response of chimneys. The following conclusions can be drawn:

(1) The d-TMISs are demonstrated to be effective for multimode control of the seismic responses of chimneys. The superiority of d-TMISs is manifested mainly as the lightweight effect compared with the traditional d-TMDs under the target performance demand. In addition, the reduction in the displacement response of the d-TMISs employed in the chimney is better than that in the acceleration under the displacement-based demand design. To summarize, considering the lightweight effect and acceptable reduction in the responses, the d-TMISs (rather than the traditional d-TMDs) can be adopted as an available technique for seismic response reduction for both newly constructed and in-service chimneys.

(2) The proposed optimal multimode control method for the seismic responses of high-rise chimneys using d-TMISs is generally effective for achieving the target performances under different excitations. Furthermore, the responses correlated with the target modes can be reduced accurately without the involvement of other irrelevant modes. Note that the high-mode control effect may be moderately trivial according to the proposed parameter distribution pattern of d-TMISs in this study. This is mainly owing

to the relatively small additional tuned mass of the TMIS for a high mode and can be solved by modifying the parameter distribution pattern. However, a large additional tuned mass of d-TMISs can be required, and a balance between the cost and high-mode control effect should be considered. In general, the proposed optimization method can provide a reference for multi-mode control of chimneys with d-TMISs and is likely to be extended to other high-rise structures.

(3) The simplification assumed for determining the parameters of d-TMISs in the optimization method is established to be reasonable with a parametric analysis involving these parameters. This facilitates the application of d-TMISs in chimneys.

There are certain limitations of the proposed multimode control design method of d-TMISs used in the chimney. A simple two-dimensional lumped mass mode is adopted for reasonable simplification in this study. It cannot provide a more detailed feedback on the chimney responses, e.g., it cannot provide information such as the stress distribution or cracking of chimney under severe earthquakes. This can be realized by developing a precise finite element model of a chimney for analysis. The soil-structure interaction is not considered for the chimney, which may affect the performance of a structure with d-TMISs. The proposed multimode control of chimney using d-TMISs can be adopted for a chimney with a flexible foundation by modifying the chimney model considering an additional soil model and their interactions. In addition, only a specific type of inerter subsystem included in the TMIS is investigated in this study. However, the proposed multimode control optimization can provide a framework for researching TMISs composed of other inerter subsystems, which deserves further study.

CRediT authorship contribution statement

Li Zhang: Methodology, Investigation, Software, Writing - original draft, Writing - review & editing, Formal analysis, Writing - original draft, Validation, Visualization. **Songtao Xue:** Methodology, Investigation, Writing - review & editing, Funding acquisition, Validation, Visualization. **Ruifu Zhang:** Conceptualization, Methodology, Writing - original draft, Writing - review & editing, Funding acquisition, Validation, Visualization. **Liyu Xie:** Writing - review & editing, Validation, Visualization. **Linfei Hao:** Funding acquisition, Validation, Visualization.

Declaration of Competing Interest

The authors declare that they have no known competing financial interests or personal relationships that could have appeared to influence the work reported in this paper.

Acknowledgements

This study was supported by the National Natural Science Foundation of China (No. 51978525, 51908156, and 51778490), the Japan Society for Promotion of Science (No. 18K04438, 19F19777), and the Science and Technology Planning Project of Guangdong Province, China (No. 2018B02028003).

Appendix A

.

Table A1
Notations.

Notations	Definition
F_{in}	Output force of two-terminal inerter element
F_s	Output force of TVMD subsystem adopted in TMIS
F_t	Total output force of TMIS
$k_{t,i}$	Stiffness of tuning spring of the i^{th} TMIS
$k_{s,i}$	Stiffness of spring element in TVMD of the i^{th} TMIS used for the i^{th} mode control
$c_{d,i}$	Damping coefficient of the i^{th} TMIS used for the i^{th} mode control
$m_{in,i}$	Inertance of the inerter element of the i^{th} TMIS used for the i^{th} mode control
$m_{t,i}$	Tuned mass of the i^{th} TMIS used for the i^{th} mode control
$x_{t,i}$	Displacement of the tuned mass of the i^{th} TMIS used for the i^{th} mode control
$x_{s,i}$	Displacement of node between the spring and inerter element of the i^{th} TMIS used for the i^{th} mode control
$\boldsymbol{M}_{\text{p}}$, $\boldsymbol{C}_{\text{p}}$,$\boldsymbol{K}_{\text{p}}$	Condensed mass, damping, and stiffness matrices, respectively, of uncontrolled chimney
$\boldsymbol{x}$, $\dot{\boldsymbol{x}}$,$\ddot{\boldsymbol{x}}$	Vectors of the displacement, velocity, and acceleration, respectively, of uncontrolled chimney
$\boldsymbol{\iota}_{\text{p}}$	Influence coefficient vector of uncontrolled chimney
$\ddot{x}_g$	Acceleration of ground motion
m_k	Lumped mass at the k^{th} node of chimney model
$\boldsymbol{M}$, $\boldsymbol{C}$,$\boldsymbol{K}$	Mass, damping, and stiffness matrices, respectively, of chimney with d-TMISs
$\boldsymbol{M}_{\text{g}}$	Mass matrix corresponding to ground motions for chimney with d-TMISs
$\boldsymbol{X}$, $\dot{\boldsymbol{X}}$,$\ddot{\boldsymbol{X}}$	Vectors of the displacement, velocity, and acceleration, respectively, of chimney with d-TMISs
$\boldsymbol{\iota}$	Influence coefficient vector of chimney with d-TMISs
$\boldsymbol{\chi}_i$	Column vector representing the location of the i^{th} TMIS
$\boldsymbol{x}_s$	State vector of the nodal displacements and velocities of chimney with d-TMISs
z_s	Response variables vector
$\boldsymbol{A}_s$, $\boldsymbol{E}_s$,$\boldsymbol{C}_s$	State-space matrices used in the state-space equation
$\boldsymbol{P}$	Covariance matrix of$\boldsymbol{x}_s$
$\boldsymbol{K}_z$	Covariance matrix ofz_s
$\boldsymbol{n}_j$	Position indication column vector of the j^{th} response variable
$S(\Omega)$	Power spectral density of the excitation with frequencyΩ
$\sigma^2_{z,j}$	Variance of the j^{th} output response variable
$\mu_{t,i}$	Equivalent mass ratio of the i^{th} TMIS used for the i^{th} mode control
$\mu_{in,i}$	Inertance to tuned mass ratio of the i^{th} TMIS used for the i^{th} mode control
$\lambda_{s,i}$	Corner frequency ratio of the i^{th} TMIS used for the i^{th} mode control
$\lambda_{t,i}$	Nominal natural frequency ratio of the i^{th} TMIS used for the i^{th} mode control
$\xi_{d,i}$	Nominal damping ratio of the i^{th} TMIS used for the i^{th} mode control
$M_{eq,i}$	Modal mass of the i^{th} mode of chimney
$\boldsymbol{\varphi}_{normal,i}$	Normalized i^{th} modal vector
$\omega_{s,i}$	Nominal circular frequency of TVMD of the i^{th} TMIS used for the i^{th} mode control
$\omega_{t,i}$	Nominal circular frequency of the i^{th} TMIS used for the i^{th} mode control
ω_i	Natural frequency of the i^{th} mode of uncontrolled chimney
$\tilde{m}_t$	Generalized mass of d-TMISs
$\tilde{\xi}_d$	Generalized nominal damping ratio of d-TMISs
ψ_i	Normalized nodal displacement of chimney
β	Parameter correlation index
$\sigma_{z0,i}$	RMS value of the displacement of the node attached by the i^{th} TMIS of uncontrolled chimney
$\sigma_{z,N}$, $\sigma_{z0,N}$	RMS values of top displacement of chimney with d-TMISs and uncontrolled chimney
γ_N	Top displacement response reduction index
$m_{t,\text{total}}$	Total tuned mass of additional d-TMISs
M_{total}	Total mass of uncontrolled chimney
$\{\Delta_{d,i}\}$	Relative displacement vector of d-TMISs
$\gamma_{N,lim}$	Target top displacement response reduction index
$\{\Delta_{d,i}\}_{lim}$	Target relative displacement vector
$\tilde{\mu}_{t,min}$, $\tilde{\mu}_{t,max}$	Lower and upper bounds, respectively, of generalized mass

(*continued on next page*)

Table A1 (*continued*)

Notations	Definition
$\tilde{\xi}_{d,min}$, $\tilde{\xi}_{d,max}$	Lower and upper bounds, respectively, of generalized nominal damping ratio
α	Safety redundancy coefficient of relative displacement of d-TMISs
$\gamma_{N,\text{peak}}$	Peak top displacement response reduction index
$\gamma_{\Delta_d,i}$	Relative displacement reduction index
α_T	Tuned mass reduction ratio
$H(\Omega)$	Frequency response function
γ_R	Top relative deflection reduction ratio
γ_A	Top acceleration reduction ratio
γ_M	Base moment reduction ratio

References

[1] CICIND. Model code for concrete chimneys, Part A: the shell. Switzerland: Committee on Industrial Chimneys 1998.
[2] ACI. 307. Standard practice for the design and construction of cast in place reinforced concrete chimneys. Michigan: American Concrete Institute 1995.
[3] Elias S, Matsagar V, Datta TK. Effectiveness of distributed tuned mass dampers for multi-mode control of chimney under earthquakes. Eng Struct 2016;124:1–16.
[4] Zhou C, Zeng X, Pan Q, Liu B. Seismic fragility assessment of a tall reinforced concrete chimney. Struct Design Tall Spec Build 2015;24(6):440–60.
[5] Zembaty Z. On the reliability of tower-shaped structures under seismic excitations. Earthq Eng Struct Dyn 1987;15(6):761–75.
[6] Huang W, Gould PL, Martinez R, Johnson GS. Non-linear analysis of a collapsed reinforced concrete chimney. Earthq Eng Struct Dyn 2004;33(4):485–98.
[7] Perrone D, Calvi PM, Nascimbene R, Fischer EC, Magliulo G. Seismic performance of non-structural elements during the 2016 Central Italy earthquake. Bull Earthq Eng 2019;17(10):5655–77.
[8] Bonkowski P, Zembaty Z, Minch MY. Time history response analysis of a slender tower under translational-rocking seismic excitations. Eng Struct 2018;155:387–93.
[9] Kilic SA, Sozen MA. Evaluation of effect of August 17, 1999, Marmara earthquake on two tall reinforced concrete chimneys. ACI Struct J 2003;100(3):357–64.
[10] Kim S, Shiohara H. Dynamic response analysis of a tall RC chimney damaged during 2007 Niigata-ken Chuetsu-oki earthquake. In: The 15th World Conference on Earthquake Engineering. Lisbon, Portugal, 2012.
[11] Wilson JL. Earthquake response of tall reinforced concrete chimneys. Eng Struct 2003;25(1):11–24.
[12] Brownjohn JMW, Carden EP, Goddard CR, Oudin G. Real-time performance monitoring of tuned mass damper system for a 183m reinforced concrete chimney. J Wind Eng Ind Aerodyn 2010;98(3):169–79.
[13] Longarini N, Zucca M. A chimney's seismic assessment by a tuned mass damper. Eng Struct 2014;79:290–6.
[14] Huang W, Gould PL. 3-D pushover analysis of a collapsed reinforced concrete chimney. Finite elem anal design 2007;43(11):879–87.
[15] Gould PL, Huang W. Higher mode effects in the nonlinear static analysis of a collapsed chimney. In: Structures Congress 2006. Missouri, USA, 2006.
[16] Elias S, Matsagar V, Datta TK. Along-wind response control of chimneys with distributed multiple tuned mass dampers. Struct Control Health Monit 2019;26:e2275.
[17] Wong KK, Johnson J. Seismic energy dissipation of inelastic structures with multiple tuned mass dampers. J Eng Mech 2009;135(4):265–75.
[18] Rana R, Soong TT. Parametric study and simplified design of tuned mass dampers. Eng Struct 1998;20(3):193–204.
[19] Pan C, Zhang RF, Luo H, Li C, Shen H. Demand-based optimal design of oscillator with parallel-layout viscous inerter damper. Struct Control Health Monit 2018;25(1):e2051.
[20] Zhao ZP, Zhang RF, Pan C, Chen QJ, Jiang YY. Input energy reduction principle of structures with generic tuned mass damper inerter. Struct Control Health Monit 2020;e2644..
[21] Ikago K, Saito K, Inoue N. Seismic control of single-degree-of-freedom structure using tuned viscous mass damper. Earthq Eng Struct Dyn 2012;41(3):453–74.
[22] Ye K, Shu S, Hu L, Zhu H. Analytical solution of seismic response of base-isolated structure with supplemental inerter. Earthq Eng Struct Dyn 2019;48:1083–90.
[23] Cao L, Li C, Chen X. Performance of multiple tuned mass dampers-inerters for structures under harmonic ground acceleration. Smart Struct Syst 2020;26:49–61.
[24] Masri SF, Caffrey JP, Li H. Transient response of MDOF systems with inerters to nonstationary stochastic excitation. J Appl Mech 2017;84(10):101003.
[25] Makris N, Moghimi G. Displacements and forces in structures with inerters when subjected to earthquakes. J Struct Eng 2019;145(2):04018260.
[26] Radu A, Lazar IF, Neild SA. Performance-based seismic design of tuned inerter dampers. Struct Control Health Monit 2019;26(5):e2346.
[27] Zhao ZP, Chen QJ, Zhang RF, Pan C, Jiang YY. Optimal design of an inerter isolation system considering the soil condition. Eng Struct 2019;196:109324.
[28] Asai T, Watanabe Y. Outrigger tuned inertial mass electromagnetic transducers for high-rise buildings subject to long period earthquakes. Eng Struct 2017;153:404–10.
[29] Zhang RF. Seismic response analysis of base-isolated vertical tank. Shanghai: Tongji University; 2014.
[30] Luo H, Zhang RF, Weng DG. Mitigation of liquid sloshing in storage tanks by using a hybrid control method. Soil Dyn Earthq Eng 2016;90:183–95.
[31] Jiang YY, Zhao ZP, Zhang RF, De Domenico D, Pan C. Optimal design based on analytical solution for storage tank with inerter isolation system. Soil Dyn Earthq Eng 2020;129:105924.
[32] Zhang RF, Zhao ZP, Dai KS. Seismic response mitigation of a wind turbine tower using a tuned parallel inerter mass system. Eng Struct. 2019;180:29–39.
[33] Sarkar S, Fitzgerald B. Vibration control of spar-type floating offshore wind turbine towers using a tuned mass-damper-inerter. Struct Control Health Monit 2020;27(1):e2471.
[34] Xu K, Bi K, Han Q, Li X, Du X. Using tuned mass damper inerter to mitigate vortex-induced vibration of long-span bridges: Analytical study. Eng Struct 2019;182:101–11.
[35] Pan C, Zhang RF. Design of structure with inerter system based on stochastic response mitigation ratio. Struct Control Health Monit 2018;25(6):e2169.
[36] Kawamata S. Development of a vibration control system of structures by means of mass pumps. Tokyo, Japan: Institute of Industrial Science, University of Tokyo; 1973.
[37] Kawamata S, Funaki N, Itoh Y. Passive control of building frames by means of liquid dampers sealed by viscoelastic material. In: The 12th World Conference on Earthquake Engineering. Auckland, New Zealand, 2000.
[38] Saito K, Toyota K, Nagae K, Sugimura Y, Nakano T, Nakaminam IS, et al. Dynamic loading test and its application to a high-rise building of viscous damping devices with amplification system. In: Third World Conference on Structural Control. Como, Italy; 2002.
[39] Ikago K, Sugimura Y, Saito K, Inoue N. Modal response characteristics of a multiple-degree-of-freedom structure incorporated with tuned viscous mass dampers. J Asian Archit Build Eng 2012;11(2):375–82.
[40] Barredo E, Blanco A, Colin J, Penagos VM, Abundez A, Gerardo Vela L, et al. Closed-form solutions for the optimal design of inerter-based dynamic vibration absorbers. Int J Mech Sci 2018;144:41–53.
[41] Zhang RF, Zhao ZP, Pan C, Ikago K, Xue ST. Damping enhancement principle of inerter system. Struct Control Health Monit 2020;e2523..
[42] Lazar I, Neild S, Wagg D. Using an inerter-based device for structural vibration suppression. Earthq Eng Struct Dyn 2014;43(8):1129–47.
[43] Xue S, Kang J, Xie L, Zhang R, Ban X. Cross-layer installed cable-bracing inerter system for MDOF structure seismic response control. Appl Sci 2020;10(17):5914.
[44] Zhao ZP, Zhang RF, Wierschem NE, Jiang YY, Pan C. Displacement mitigation-oriented design and mechanism for inerter-based isolation system. J Vib Control 2020.
[45] Krenk S. Resonant inerter based vibration absorbers on flexible structures. J Franklin Inst 2019;356(14):7704–30.
[46] Javidialesaadi A, Wierschem NE. Optimal design of rotational inertial double tuned mass dampers under random excitation. Eng Struct 2018;165:412–21.
[47] Garrido H, Curadelli O, Ambrosini D. Improvement of tuned mass damper by using rotational inertia through tuned viscous mass damper. Eng Struct 2013;56:2149–53.
[48] Chen QJ, Zhao ZP, Xia Y, Pan C, Luo H, Zhang RF. Comfort based floor design employing tuned inerter mass system. J Sound Vib 2019;458:143–57.
[49] De Domenico D, Ricciardi G. Improving the dynamic performance of base-isolated structures via tuned mass damper and inerter devices: A comparative study. Struct Control Health Monit 2018;25:e2234.
[50] Zhao ZP, Zhang RF, Jiang YY, Pan C. A tuned liquid inerter system for vibration control. Int J Mech Sci 2019;164:105171.
[51] Chen QJ, Zhao ZP, Zhang RF, Pan C. Impact of soil-structure interaction on structures with inerter system. J Sound Vib 2018;433:1–15.
[52] Lutes LD, Sarkani S. Stochastic analysis of structural and mechanical vibrations. Upper Saddle River, NJ: Prentice Hall; 1997.
[53] Chankong V, Haimes YY. Multiobjective decision making: theory and methodology. New York: Elsevier; 1983.
[54] Palermo M, Silvestri S, Gasparini G, Trombetti T. Seismic modal contribution factors. Bull Earthq Eng 2015;13(10):2867–91.
[55] Chopra AK. Dynamics of structures: theory and applications to earthquake engineering. Englewood Cliffs(NJ): Prentice; 1995.
[56] Aardal K, Nemhauser GL, Weismantel R. Handbooks in Operations Research and Management Science: Discrete Optimization. New York: Elsevier; 2005.
[57] Liang S, Yang W, Song J, Wang L, Hu G. Wind-induced responses of a tall chimney by aeroelastic wind tunnel test using a continuous model. Eng Struct 2018;176:871–80.
[58] GB 50011-2010. Code for seismic design of buildings. Beijing: the Ministry of Housing and Urban-Rural Construction of the People's Republic of China; 2010.
[59] GB 50051-2013. Code for design of chimneys. Beijing: the Ministry of Housing and Urban-Rural Construction of the People's Republic of China; 2013.
[60] PEER. PEER ground motion database. Pacific Earthquake Engineering Research Center 2020.
[61] Pan C, Zhang RF, Luo H, Shen H. Target-based algorithm for baseline correction of inconsistent vibration signals. J Vib Control 2018;24(12):2562–75.
[62] Den Hartog JP. Mechanical vibrations. Dover (NY): McGraw-Hill; 1956.